Semi-arid zone caves

Markowska, Monika; Baker, Andy; Andersen, Martin S.; Jex, Catherine N.; Cuthbert, Mark O.; Rau, Gabriel C.; Graham, Peter W.; Rutlidge, Helen; Mariethoz, Gregoire; Marjo, Christopher E.; Treble, Pauline C.; Edwards, Nerilee

DOI:
10.1016/j.quascirev.2015.10.024

Semi-arid zone caves: Evaporation and hydrological controls on $\delta^{18}O$ drip water composition and implications for speleothem paleoclimate reconstructions.

[*1,2]Monika Markowska, [2]Andy Baker, [4]Martin S. Andersen, [2]Catherine N. Jex, [3,4]Mark O. Cuthbert, [4]Gabriel C. Rau, [2]Peter W. Graham, [2,5]Helen Rutlidge, [2,6]Gregoire Mariethoz, [5]Christopher E. Marjo, [1]Pauline C. Treble, [7]Nerilee Edwards

[1]*Institute for Environmental Research, Australian Nuclear Science and Technology Organisation, Lucas Heights, Sydney 2234, Australia.*

[2]*Connected Waters Initiative Research Centre, UNSW Australia, Kensington, Sydney 2033, Australia.*

[3]*School of Geography, Earth and Environmental Sciences, University of Birmingham, Edgbaston, Birmingham, B15 2TT, UK*

[4]*Connected Waters Initiative Research Centre, UNSW Australia, 110 King Street, Manly Vale, NSW 2093, Australia*

[5]*Solid State and Elemental Analysis Unit, Mark Wainwright Analytical Centre, UNSW Australia, Kensington, NSW, Australia 2052*

[6]*Institute of Earth Surface Dynamics (IDYST), University of Lausanne, Geopolis, 1015 Lausanne, Switzerland.*

[7]*Douglas Partners Pty Ltd, 96 Hermitage Road West Ryde, New South Wales, 2114, Australia.*

*Corresponding author: Monika Markowska. Permanent address: Institute for Environmental Research, Australian Nuclear Science and technology Organisation, New Illawarra Road, Lucas Heights, Sydney, NSW 2234. Ph: +61 2 9717 9313.

Email Addresses: Monika Markowska: Monika.Markowska@ansto.gov.au, Andy Baker: a.baker@unsw.edu.au, Martin S. Andersen: m.andersen@unsw.edu.au, Catherine N. Jex c.jex@unsw.edu.au, Peter W. Graham p.w.graham@student.unsw.edu.au, Mark O. Cuthbert: m.cuthbert@unsw.edu.au, Gabriel C. Rau: gabriel.rau@unsw.edu.au, Helen Rutlidge h.rutlidge@unsw.edu.au, Chistopher E. Marjo c.marjo@unsw.edu.au, Gregoire Mariethoz gregoire.mariethoz@unsw.edu.au, Pauline C. Treble: Pauline.Treble@ansto.gov.au, Nerliee Edwards Nerilee.Edwards@douglaspartners.com.au

Abstract

Oxygen isotope ratios in speleothems may be affected by external processes that are independent of climate, such as karst hydrology and kinetic fractionation. Consequently, there has been a shift towards characterising and understanding these processes through cave monitoring studies, focussing on temperate zones where precipitation exceeds evapotranspiration. Here we investigate oxygen isotope systematics at Wellington Caves in semi-arid, SE Australia where evapotranspiration exceeds precipitation. We use a novel D_2O isotopic tracer in a series of artificial irrigations, supplemented by pre-irrigation data comprised four years of drip monitoring and three years of stable isotope analysis of both drip waters and rainfall. This study reveals that: (1) evaporative processes in the unsaturated zone dominate the isotopic composition of drip waters; (2) significant soil zone 'wetting up' is required to overcome soil moisture deficits in order to achieve infiltration, which is highly dependent on antecedent hydro-climatic conditions; (3) lateral flow, preferential flow and sorption in the soil zone are important in redistributing subsurface zone water; (4) isotopic breakthrough curves suggest clear evidence of piston-flow at some drip sites where an older front of water discharged prior to artificial irrigation water; and (5) water residence times in a shallow vadose zone (<2 m) are highly variable and can exceed six months. Oxygen isotope speleothem records from semi-arid regions are therefore more likely to contain archives of alternating paleo-aridity and paleo-recharge, rather than paleo-rainfall i.e. the amount effect or mean annual. Speleothem-forming drip waters will be dominated by evaporative enrichment, up to ~3‰ in the context of this study, relative to precipitation-weighted mean annual rainfall. The oxygen isotope variability of such coeval records may further be influenced by flow path and storage in the unsaturated

zone that is not only drip specific but also influenced by internal climatic conditions, which may vary spatially in the cave.

1. Introduction

Speleothems have been utilised as valuable records of palaeoenvironmental change in many climatic zones (e.g. Wang et al., 2001; Cruz et al., 2005; Henderson, 2006; Baker et al., 2015). However, speleothem records are influenced by their depositional environment (Fairchild and Baker, 2012), for example, karst hydrological flow path routing that can affect the chemical and isotopic composition of speleothem-forming drip waters (Tooth and Fairchild, 2003; Fuller et al., 2008; Verheyden et al., 2008; Pape et al., 2010; Treble et al., 2013, Lou et al., 2014). Interpreting speleothems to understand Quaternary climate variability therefore necessitates an understanding of speleothem formation processes, which requires site-specific in situ cave monitoring. There are many Quaternary speleothem paleoclimate records from semi-arid/water-limited areas (Burns et al., 2002; Vaks et al., 2010; Denniston et al., 2013); however, there are few karst hydrological studies, e.g. Soreq Cave (Bar-Matthews et al., 1996; Ayalon et al., 1998), from these often remote locations. As a result important factors such as water balance (i.e. recharge, evapotranspiration loss) and spatial variability are still poorly constrained. This study aims to improve constraints on hydrological flow dynamics and their influence on $\delta^{18}O$ drip water composition in semi-arid karst regions, and by extension, identify the potential implications for speleothem records.

1.1 Semi-arid zone karst hydrology

Arid and semi-arid regions cover approximately one third of the world's total land surface (McKnight and Hess, 2000), and generally lie between the latitudes of 10 – 35°, poleward of the Inter-Tropical Convergence Zone (Lansberg and Schloemer,

1967). Aridity can be described as a moisture shortage, primarily dictated by long-term regional climatic conditions (Agnew and Anderson, 1992). The most common measure of aridity is the Aridity Index, which is the ratio of water input (precipitation, P) and water loss (potential evapotranspiration, PET). Semi-arid areas have an aridity index between 0.2 and 0.5 (UNEP, 1992).

Groundwater recharge, the downward flow of water adding to groundwater storage (Healy, 2010), is strongly influenced by climate, geology, vegetation, solar radiation, soils and geomorphology which control recharge processes (Freeze and Cherry, 1979). In semi-arid regions, surface processes such as rainfall and evapotranspiration tend to be much more important in governing groundwater recharge amount and frequency. Rainfall in the Australian semi-arid zone is typically infrequent and highly episodic, marked with multi-annual droughts, and punctuated by periods of above average rainfall and flooding. As a result, the annual groundwater recharge can be low; for example, Allison and Hughes (1983) suggest groundwater recharge is less than 10 mm/a in semi-arid SE Australia. In temperate zones recharge tends to occur predominately in a diffuse (sometimes known as 'direct') manner. As aridity increases, diffuse recharge is generally less frequent as PET regularly exceeds rainfall, and effective recharge relies heavily on high magnitude rainfall events to overcome existing soil moisture deficits (de Vries and Simmers, 2002). Where ET varies seasonally this may bias recharge to cooler months, with lower ET, when soil moisture deficits are more easily overcome (Walton, 1969).

In semi-arid regions, percolation from surface features such as rivers, streams and lakes to groundwater, known as 'focused' or 'indirect' recharge, are thought to be more prevalent than direct recharge (Healy, 2010). However, there are at least two

reasons why this generalisation is not necessarily true in semi-arid karst areas. Firstly, soils are often thin, potentially limiting the impact of soil moisture deficits in preventing recharge compared to areas with thicker soils, where larger soil moisture deficits may accumulate. Secondly, recharge in fractured rock environments is commonly associated with significant preferential flow, along paths such as fractures and fingers of enhanced wetness, bypassing the soil profile and unsaturated zone (Cuthbert et al., 2013). Thus, recharge may be highly variable both spatially and temporally in these environments (Cuthbert and Tindimugaya, 2010).

Karst hydrology is highly heterogeneous due to fractures, fissures and bedding planes enlarged by carbonate dissolution, which permit rapid water movement through the unsaturated zone, via preferential flow, potentially minimising the time for evapotranspiration losses. Water movement and storage potential in karst are highly dependent on porosity, the ratio between the volume of voids and the total volume of the porous medium and permeability, the capacity of the porous rock to transmit water. For karst, there are typically three types of porosity: primary (mainly intergranular or matrix), secondary (fracture or fissure flow) and tertiary (conduit flow) (Ford and Williams, 2007). Porosity is shown to be approximately exponential with aquifer age and can serve as a proxy for the degree of mesogenetic diagenesis (Florea and Vacher, 2006). Telogenetic limestone typically has negligible primary porosity (0-3%) due to porosity reduction through past burial diagenesis (Ford and Williams, 2007; Vacher and Mylorie, 2002), thus most water is transmitted via fracture networks or conduit flow. In contrast, eogenetic limestone, which has not undergone burial, has significantly higher matrix permeability (Vacher and Mylorie, 2002; Treble et al., 2013).

Within the karst bedrock itself there is also variation in water movement and storage potential. The epikarst is a term commonly used to describe the upper layers of the carbonate bedrock, directly beneath soil and regolith if present (Williams, 2008). It is considered a zone of storage rather than transmission, with higher secondary permeability and porosity (10-30%; Williams, 2008) in comparison to the bulk rock below (Klimchouk, 2004). Secondary permeability and porosity are those that developed in the rock after deposition and result due to processes such as weathering, fracturing and dissolution. Thus, the epikarst may function as a perched aquifer, with considerable lateral water flow (e.g. via bedding planes), before water eventually percolates downwards (Jones, 2013). The rock below the epikarst typically has considerably less secondary porosity and permeability and rather acts as a transmission zone, along smaller flow paths or less concentrated larger fractures, eventually redistributing the stored epikarst waters above to the karst aquifer. Due to its role in water storage, the epikarst is assumed to play a major part in mixing of waters of different ages (Aquilina et al., 2006; Clemens et al., 1999; Perrin et al., 2003; Oster et al., 2012) as well as chemical dissolution (Jones, 2006).

Water residence times from infiltration to drip waters vary, e.g. ranging from 1-3 months (southern France; Aquilina et al., 2005), and up to 26–36 years (Israel; Kaufman et al. 2003). This inherent heterogeneity in the spatial distribution of water in the unsaturated zone together with climate makes the estimation of recharge fluxes and soil moisture balance in karst semi-arid zone regions difficult and associated with high uncertainty.

1.2 Stable isotopic composition of karst drip waters

Stable isotopes, such as oxygen isotopes, are important tools in understanding global water cycles. $\delta^{18}O$ is also the most commonly used proxy in paleoclimate reconstructions from speleothems. Measurements of drip water $\delta^{18}O$ values help us understand water balance processes in the unsaturated zone relative to the rainfall input and hence may be used to characterise drip water $\delta^{18}O$ as a climate proxy as well as to identify flow pathways and mixing above the cave (Yonge et al., 1985; Ayalon et al., 1998; Williams and Fowler, 2002; Perrin et al., 2003; Cruz et al., 2005; van Beynen and Febbroriello, 2006; Fuller et al., 2008; Onac et al, 2008; Pape et al., 2010; Baldini et al., 2008; Treble et al. 2013; Lou et al., 2014).

Precipitation and groundwater isotope samples generally fall close to the Global Meteoric Water Line (GMWL), defined as $\delta D = 8(\delta^{18}O) + 10$ ‰ (Craig, 1961), which is determined by the ratio of $\delta D/\delta^{18}O$ under equilibrium fractionation factors (Sharp, 2007). Phase changes such as evaporation and condensation between water and its vapour, fractionate both $\delta^{18}O$ and δD, but in 100% relative humidity conditions isotopes in water and air phases approach isotopic equilibrium (Gonfiantini, 1986). However, in <100% relative humidity conditions, a humidity gradient between the water surface and air boundary causes diffusion across this layer, resulting in a net evaporation flux (evaporation into an unsaturated atmosphere) (Gat, 1996). This kinetic fractionation is a direct function of the prevailing relative humidity and was estimated by Gonfinatini (1986). In semi-arid environments the net evaporative flux often results in the systematic isotopic enrichment of water. Thus, slopes of $\delta^{18}O$ and δD, which ordinarily sit on a GMWL with a slope of 8, are typically lower or on a Local Meteoric Water Line (LMWL) (Gat, 1996). Seasonal variations in slope are dependent on; water temperature, humidity, and the isotopic separation between the annual precipitation and the evaporation-flux weighed atmospheric moisture

(Dansgaard, 1964; Gibson et al., 2008). Water stored in upper soil layers is often more enriched with reported slopes <3 (Gibson et al., 2008). However, as evaporation is a dominant soil process most of the water volume is likely to be lost, thus infiltration to the vadose zone is likely to be negligible (Cuthbert et al., 2014a).

Evaporative enrichment of water in the unsaturated zone of semi-arid karst environments measured as drip waters has been reported, for example: $\delta^{18}O$ +1.5‰ (Bar-Matthews et al., 1996) and up to +2.7‰ (Cuthbert et al., 2014a). The karst hydrology has been demonstrated to be an important controlling factor where enrichment was shown to vary with drip type, where slower more diffuse drips showed a larger offset ($\delta^{18}O$ +1 to +1.5‰) than faster drips (+0.5‰) (Ayalon et al., 1998). In contrast, drip waters isotopically-depleted relative to rainfall have also been interpreted indicating preferential infiltration from large, ^{18}O-depleted storm events suggesting infiltration thresholds (Jones and Banner, 2003; Pape et al., 2010). However, karst hydrology studies in semi-arid zones are few and there is likely to be substantial intra- and inter-site variability between hydrological behaviour in the unsaturated zone of karst environments, which can only be quantified by site-specific in situ monitoring.

1.3 In situ cave monitoring

In situ drip monitoring in caves can inform about water movement in the karst unsaturated zone. Early methods of characterising drip hydrology came from the deployment of automatic tipping buckets under dripping stalactites (Gunn, 1974). More recently, Stalagmates® are designed to count individual drips (Collister and Mattey, 2008). Drip monitoring can be used to characterize karst flow regimes, e.g. slow seepage flow vs. fast fracture flow, for individual sites in the cave system (Smart

and Freiderich, 1986; Jex et al., 2012; Markowska et al. 2015). Non-linearity in cave discharge responses have been observed (Baker et al., 1997; Baker and Brundson, 2003), which must be due to the inherent physical spatial heterogeneity and temporal dynamics of flow processes in the karst system (Labat et al., 2000; Labat et al., 2002). This is likely to be enhanced in semi-arid environments where soil moisture deficits typically need to be overcome in order to activate cave drip discharge.

Tracer techniques are one of the most useful tools in understanding water residence times, flow and mixing in hydrological systems. However, despite its great potential, using water labelled with deuterium is still relatively uncommon especially in unsaturated zone systems (Koeniger et al., 2009). In this study, we have used natural stable water isotopes as a tracer to understand the hydrological flow in SE Australia, expanding on a baseline dataset published in Cuthbert et al., (2014a). The aim of this study is to better constrain the flow dynamics, identify the main drivers controlling oxygen isotope composition and assess how this may impact speleothem-based paleoclimate reconstructions in semi-arid zones regions. No speleothem records exist yet for this region.

The study site Cathedral Cave (CC) was chosen as it is already well characterised and processes such as: karst hydrology (Jex et al., 2012; Mariethoz et al., 2012), isotopic drip water evolutions in the unsaturated zone (Cuthbert et al. 2014a), and drip water geochemistry (Rutlidge et al., 2014, Rutlidge et al., 2015) have previously been described. Additionally, two studies by Cuthbert et al. (2014b) and Rau et al. (2015) investigate cave air and drip water temperature dynamics, demonstrating significant evaporative cooling even under conditions of high relative humidity. The data presented in the latter four publications has been generated from the same irrigation

experiments presented in this paper. Here, we present the isotopic drip water data and drip rate responses during a series of artificial irrigations. Our irrigation experiments were designed to replicate natural precipitation events, overcoming the soil moisture deficit and thus provoking a drip water response. They were applied directly over a small focused irrigation area above a shallow cave chamber in order to increase the likelihood of drip response in the cave below. The tracer injection was designed to exaggerate the natural isotopic drip water responses to better understand hydrological processes and the resultant isotopic evolution of speleothem-forming drip waters.

2. Study Site: Wellington, NSW

The study site, CC, is located in SE New South Wales, Australia (32°37´S; 148°56´E) (Figure 1). It is approximately 8 km south of the town of Wellington to the west of the Great Dividing Range, on the plains at approximately 300 m asl (above sea level). PET (~1200 mm/a) greatly exceeds annual mean precipitation (~600 mm/a) causing long-lasting soil moisture deficits and hence only sporadic recharge events reach the cave and deeper groundwater system (Cuthbert et al. 2014a). Episodic high intensity rainfall due to large convective storms are experienced in this part of SE Australia (Kuleshov et al., 2012), although these tend not to cause recharge. Rather, it is the stationary weather systems, typically a high level trough from the tropical north interacting with a low level system (i.e., a cut-off low or front from the west), which maintains rainfall for prolonged periods of time and results in recharge. Jex et al. (2012) quantified that precipitation resulting in recharge must be at least ~60 mm within a 24-48 hour period, but is variable depending on soil moisture antecedent conditions. No surface water flows across the site, and overland flow is rarely (if ever) observed. Median rainfall is approximately uniform year round (BOM, 2014).

Wellington has an aridity index of 0.5 and thus falls within UNEP's (1992) semi-arid definition. Annual surface air temperature ranges from ~0 to ~45°C and an annual maximum mean temperature of 24.3°C (Rau et al., 2015).

Annual cave air temperature ranges from 15 to 18 °C, whilst deeper sections of the cave (i.e., site 3) remain relatively constant at 17.8°C (Rau et al., 2015). Variable cave air temperatures exist closer to the entrance due to air exchange (venting) from pressure and density effects (Cuthbert et al., 2014b; Rau et al., 2015). Enhanced air exchange closer to the surface is also reflected in reported relative humidity values, where near-entrance sites varied considerably over time, with minimum, maximum and median values of 59.3%, 97.9% and 88.6%, respectively (Rau et al., 2015). Deeper in the cave, only minimal fluctuations in relative humidity were measured, with minimum, maximum and median values of 96.5%, 97.1% and 97.8%, respectively (Rau et al., 2015). Cuthbert et al. (2014b) and Rau et al. (2015) identified significant in-cave evaporation, resulting in drip water cooling, which is most prevalent at near-entrance areas of the cave.

CC was formed in the Devonian Garra Formation limestone and the regional geomorphology has been extensively studied and is described in Osborne et al. (2007). The cave has two entrances, one major and one minor, located at 325 m asl, which descend approximately 25 m, ending at a flooded passage which intercepts the water table (Cuthbert et al., 2014a). The water level in the passage is variable, and dependent on the prevailing climatic conditions. For example, in 2010 at the beginning of a strong La Niña phase, which brought large rainfalls to the region, CC flooded (from this passage upwards) due to a rise in the water table. The Devonian limestone is present in two distinct types, it is thinly bedded in the mid cave section,

264 westerly dipping at 70°, and marmorised in all other areas of the cave, e.g., at study
265 sites 1, 2 and 3 (Figure 1). The cave morphology has further been described in Jex et
266 al. (2012) and Cuthbert et al. (2014b). The hydrology from some drip sites from site 3
267 have been previously described in Jex et al. (2012) (sites: 369, 321, 325, 329, 332,
268 342, 348, 372, 395, 396, 279, 280, 357, 370, 377, 376, 379, 326 and 352) and
269 Cuthbert et al. (2014a) (sites: 319, 320, 322, 330, 380, 382 and 387). There is a thin
270 and discontinuous surface soil layer estimated to vary between 0 and 0.3 m and is
271 expected to protrude to deeper levels above fractures in the underlying bedrock
272 (Rutlidge et al., 2014).

273 # 3. Methods

274 ## 3.1 Pre-irrigation stable isotope sampling and analysis

275 Instantaneous (spot) drip water samples from CC were sampled over the period 2010-
276 2011 from three general sample zones in the cave (site 1: shallow, site 2: middle and
277 site 3: deep, see Figure 1), totalling 115 samples. Monthly-integrated drip water
278 isotope sampling began in March 2011 and continued until March 2013 from 5 drip
279 sites: 326 (same as in Jex et al., 2012), 331, 361, 364, and 385 (56 individual
280 observations) at Site 1 (Figure 1) and from site 3 as reported in Cuthbert et al.
281 (2014a). For sampling procedures see Cuthbert et al. (2014a). Monthly-integrated
282 rainfall samples were collected in accordance to the recommended protocol stipulated
283 by the International Atomic Energy Agency (IAEA) (http://www-
284 naweb.iaea.org/napc/ih/documents/userupdate/sampling.pdf) at the UNSW
285 Australia's Wellington Field Station, approximately 7 km from Cathedral Cave.

286 All water samples were stored in 28 mL glass McCartney sample bottles leaving no
287 headspace. Water samples were analysed on a Los Gatos® cavity ring down laser

spectrometer at UNSW Australia. The overall precision on analysis was ±0.12‰ $\delta^{18}O$ and ±1.2‰ δD. Enriched samples from the two irrigation experiments (2013 and 2014, see section 3.2) were associated with larger errors of ±0.15‰ $\delta^{18}O$ and ±2.0‰ δD, as results were extrapolated outside of the isotopic values of the standards. Approximately 40 samples from the 2014 irrigation experiment were analysed at the Australian Nuclear Science and Technology Organisation (ANSTO) on a Picarro cavity ring down laser spectrometer. These samples were diluted with a known internal standard AILS004 (δD = -173.93‰ ±0.54‰ and $\delta^{18}O$ = -22.19‰ ±0.02‰), calibrated against Vienna reference materials VSMOW2-SLAP2 and had errors of 2.3‰ for δD and 0.23‰ for $\delta^{18}O$. All samples were calibrated against the following ANSTO internal standards, which were calibrated against VSMOW2-SLAP2: AILS001 (δD = 32.5‰ ±0.9 ‰ and $\delta^{18}O$ = 7.47‰ ±0.02‰) AILS002 (δD = -8.0‰ ±0.8‰ and $\delta^{18}O$ = -1.41‰ ±0.05‰), AILS003 (δD = -80.0 ±0.5 and $\delta^{18}O$ = -12.16‰ ±0.04‰) and AILS004 (δD = -173.93‰ ±0.54‰ and $\delta^{18}O$ = -22.19‰ ±0.02‰).

Drip monitoring using drip loggers (Stalagmates®) counting at 15-minute intervals started at CC in 2010 (Jex et al., 2012) and is ongoing at sites 1 and 3 (Figure 1). In this study we present an expanded dataset covering the period July 2010 to June 2014, and including previously published data from Cuthbert et al., (2014a) over January 2011 to June 2013.

3.2 Irrigation experiment summary

A summary of the 2013 and 2014 irrigation experimental conditions are provided in Table 1. The 2013 irrigation experiment consisted of four irrigations over CC, over four consecutive days. The 2014 irrigation experiment consisted of three irrigations over CC, over two consecutive days. Equivalent P (mm) was calculated by converting

the total irrigation volume (L) to cubic metres, and dividing it by the total irrigation area (m^2). Net infiltration (mm) was estimated by subtracting the average daily PET for the month of January from the equivalent P, to provide an estimate of infiltration potential after evaporative losses.

Table 1. Summary of irrigation experiments during 2013 and 2014.

Irrigation number	Date	Irrigation type	Isotopic composition (‰)	Volume (L)	Equivalent P (mm)	Net infiltration (mm)	site 1: Drip response?	site 2: Drip response?	site 3: Drip response?
2013 Irrigation Experiment									
1	8/01/13	Town water with D_2O tracer	3.75 ‰ ($\delta^{18}O$), +6100 ‰ (δD)	840	~35	~28.5	N	Y	N*
2	9/01/13	Town water	-4.55 ‰ ($\delta^{18}O$), -13.6 ‰ (δD)	1500	~63	~56.5	Y	N**	N*
3	10/01/13	Town water	-4.91 ‰ ($\delta^{18}O$), -28.0 ‰ (δD)	840	~35	~28.5	Y	N**	N*
4	11/01/13	Town water	-4.55 ‰ ($\delta^{18}O$), -25.5 ‰ (δD)	1500	~63	~56.5	Y	N**	N*
2014 Irrigation Experiment									
5	14/01/14	Town water	-2.60 ‰ ($\delta^{18}O$), -20.6‰ (δD)	3400	~68	~61.5	Y	N	N*
6	15/01/14	Town water with D_2O tracer	-1.78 ‰ ($\delta^{18}O$), +6700‰ (δD)	1000	~20	~16.75	Y	N	N*
7	15/01/14	Town water	-2.35 ‰ ($\delta^{18}O$), -17.9‰ (δD)	1400	~28	~24.75	Y	N	N*

*Dripping prior to experiment.
** Dripping from previous activation, no drip response observed.

3.2.1 2013 Irrigation experiment summary

Artificial irrigations were conducted using Wellington town supply water above CC during January 2013 (Southern Hemisphere summer). Conditions were exceptionally hot and dry, with daytime temperatures exceeding 40°C which is greater than both the January mean maximum temperature (32.9°C) and 9th decile maximum temperature (37.8°C). Four artificial irrigations were conducted over a 21 m^2 area (3 x 7 m) area using two hand-held hoses, on the surface directly above CC; see Table 1 for summary and also Rutlidge et al. (2014). The soil volume is 2.1–6.3 m^3 (Rutlidge et al., 2014), equivalent to 3.8–11.3 tons (assuming a dry bulk density of 1.8 g mL^{-1}),

thus given initial soil moisture content of 0.16 wfv (assuming a field capacity of 0.6 wfv) the soil's additional water storage capacity is approximately 1890–5670 L (Rutlidge et al., 2014). In irrigation 1, 840 L of town supply water was spiked with 0.5 L 99.8% deuterium (D_2O), which was mixed in a 1600 L tank by circulating the water using a Monsoon centrifugal pump as well as manual stirring with shovels for 15 mins. This resulted in a ^2H enrichment of 6100‰ ±5.0‰ and water samples at the beginning and end of irrigation from the tank showed the tracer was well mixed. The water was then distributed over the irrigation area using two Monsoon pumps, over the irrigation area for a 3-hour period. Four individual drip points were monitored at site 1 located at approximately 5 m below the surface and included WS1, WS2, WS16 and WS21 (Figure 1). Three individual drip points were monitored at site 2, located at approximately 10 m below the surface, and include WS9, WS10 and WS11. In irrigation 2, the irrigation area was adjusted by 2-3 metres, to ensure irrigating was directly over site 1, after no dripping was observed after irrigation 1. Over irrigations 2, 3 and 4, 1500, 840 and 1500 L of town supply water was irrigated, containing no deuterium tracer. Equivalent rainfall and net infiltration were calculated (Table 1). Stable isotope samples were collected in 28 mL glass McCartney bottles every 30 mins when there was sufficient dripping to fill the entire bottle with no headspace.

3.2.2 2014 Irrigation experiment summary

During January of 2014 a second artificial irrigation experiment was conducted at CC. The weather was similar to conditions in 2013, with daytime maximum temperatures usually exceeding 40°C. Over a 2-day period, three artificial irrigations were conducted over a 50 m^2 area (5 x10 m) on the surface directly above the CC. In contrast to the 2013 irrigation, a slightly larger area was irrigated in order to activate a

353 wider range of drip sites and a ‘wetting-up’ irrigation of 3400 L without deuterium
354 tracer was included. Equivalent rainfall and net infiltration were calculated as
355 described for 2013 and shown in Table 1.

356 On the second day of irrigation (15/01/2014), fifteen evaporation pans comprised of
357 glass petri dishes (7.09^{-3} m^2) were installed. They were placed in five cave locations
358 with three replicate pans at each and deployed at depths ranging from 0 to 25 m below
359 the surface (Figure 1). Pans were placed at drip monitoring sites 1, 2 and 3, as well as
360 an additional site near the cave entrance labelled ‘Entrance’ and another between sites
361 2 and 3 labelled ‘Mid-cave’ (Figure 1). An additional pan was deployed at the surface
362 under a shaded cardboard shelter, open on all sides to provide air ventilation, to
363 simulate a low humidity evaporative environment. Pans were left overnight for
364 approximately 21 hours, except at site 3, which had low evaporation rates coupled
365 with a high RH of ~98% (Rau et al., 2015), therefore a longer time period of January
366 2014 to March 2014 was used to calculate the mean loss per day Volumetric loss of
367 water from evaporation was calculated by measuring the volume of water before and
368 after using a graduated measuring cylinder (with an error of ± 0.5 mm). The water
369 from the three pans deployed at each site were then combined and analysed for stable
370 water isotopes on a Los Gatos® cavity ring down laser spectrometer at UNSW
371 Australia.

372 ### 3.4 Statistical analyses

373 Our stable isotope data were subjected to a non-parametric Mann-Whitney U test
374 (confidence interval of 0.95) using the Monte Carlo method to produce sample
375 simulations (n = 20,000). This method was preferred over t-tests as it performs better

than the t-test for non-parametric distributions and has almost equal efficiency for normal distributions (Vickers et al., 2005).

4. Results

4.1 Pre-irrigation data

4.1.1 Climate and drip rate monitoring

A 3.5-year background of climate and drip hydrological monitoring data is presented in Figure 2. This includes the shallowest site (site 1) and the deepest (site 3). Additionally, the timing of the two irrigation experiments (January 2013 and January 2014) is indicated, the results of which will be discussed in section 4.2 onward.

The mean precipitation-weighted annual isotopic composition of rainfall from Cuthbert et al. (2014a) is δD = -23.54‰ and $\delta^{18}O$ = -4.28‰ (Figure 3). The median rainfall amount confirms that P at Wellington is not seasonal, although PET is typically enhanced in summer and reduced in winter (Figure 2); thus recharge is statistically more likely to occur during winter. At shallower site 1, dripping was quite variable, ranging from 0 to 60 drips per 15 minutes (Figure 2). Drips activated during or following significant rainfall events when field capacity was surpassed. Drainage occurred from the soil zone via fractures and fissures in the limestone epikarst, which resulted in rapid, short-lived drip responses (Figure 2). During periods of no infiltration, all drips ceased to discharge for up to several months at a time. In contrast at deeper site 3 many drips remained discharging at a base level of ~1-5 drips per 15 minutes, despite reaching up to 350 drips per 15 minutes following high rainfall (Figure 2).

4.1.2 Drip water isotope spot sampling 2010-11

Over 2010-2011 spot samples were routinely taken (n = 115) from CC at sites 1 (n = 19), 2 (n = 11) and 3 (n = 85) and the summary of stable isotope results are

shown in Table 3 and data in Figure 2. In Figure 3A δD against $\delta^{18}O$ data are shown and the regression equations (CI = 95%) calculated from these are compared with the Local Meteoric Waterline (LMWL) from Cuthbert et al. (2014a) and Global Meteoric Waterline (GMWL) in Figure 3B. Overall, mean stable isotopic compositions for all drip water δD and $\delta^{18}O$ were -21‰ and -3.9‰, respectively, which were enriched in δD and $\delta^{18}O$, by 3‰ and 0.4‰ respectively, in comparison to the mean precipitation-weighted annual rainfall composition (Figure 3A). Although average isotopic compositions of drip waters from sites 1-3 appear similar (Table 3), a Mann-Whitney U test revealed that the populations of samples from site 1 and 3 were significantly different (ρ = 0.006, α = 0.05), but only in terms of δD composition, not $\delta^{18}O$. All spot sample sites plotted on slightly different LMWL's with slopes <8 (Figure 3B). Linear regression lines for sites 1, 2 and 3 had coefficients of determination (r^2) of: 0.83, 0.49 and 0.68, respectively. Slope values were between 3.1 and 5.6, and the lowest was from site 2, although with a lower r^2, only 49% of the variation was explained.

425 **Table 3.** Summary of mean drip site water stable isotopic composition for spot samples from 2010 to
426 20111 for the three cave sites (site 1: shallow, site 2: medium, and site 3: deep, see Figure 1).

427

site ID	n	δD	SD	$\delta^{18}O$	SD	site ID	n	δD	SD	$\delta^{18}O$	SD
site 1 (- 5 m below the surface)						**site 3 (-25 m below the surface) cont.**					
C1	7	-22	2.3	-4.4	0.31	328	2	-21	nd	-4.5	nd
C2	3	-18	1.6	-3.8	0.22	329	1	-20	nd	-3.5	nd
C3	3	-17	1.9	-3.4	0.56	330	4	-20	3.1	-3.6	0.39
331	1	-17	nd	-3.5	nd	332	2	-23	nd	-4.2	nd
361	1	-14	nd	-2.6	nd	342	1	-20	nd	-3.7	nd
364	2	-16	nd	-3.6	nd	346	1	-20	nd	-3.6	nd
Total	**19**	**-19**	**3.24**	**-3.9**	**0.62**	347	1	-18	nd	-3.7	nd
Min		-24		-4.8		350	1	-18	nd	-3.4	nd
Max		-14		-2.6		352	2	-21	nd	-4.0	nd
site 2 (-10 m below the surface)						354	1	-23	nd	-4.1	nd
C5	3	-21	1.4	-3.8	0.29	355	3	-20	1.4	-3.8	0.45
C6	6	-21	0.8	-3.7	0.19	362	1	-21	nd	-3.9	nd
C7	2	-19	2.5	-3.1	0.7	366	2	-20	nd	-3.7	nd
Total	**11**	**-20**	**1.4**	**-3.6**	**0.39**	368	4	-20	0.4	-3.7	0.11
Min		-22		-4.1		370	2	-22	1.1	-4.3	0.29
Max		-17		-2.6		372	4	-21.7	1.2	-4.0	0.15
site 3 (-25 m below the surface)						374	4	-21	0.9	-4.0	0.17
C10	1	-29	nd	-5.3	nd	376	3	-23	1.5	-4.2	0.05
C12	1	-22	nd	-4.3	nd	379	2	-22	nd	-4.1	nd
C13	1	-24	nd	-4.9	nd	380	2	-22	nd	-3.9	nd
C105	1	-17	nd	-3.4	nd	382	2	-18	nd	-3.7	nd
C109	1	-24	nd	-4.0	nd	383	1	-21	nd	-4.0	nd
C110	1	-23	nd	-4.1	nd	386	1	-10	nd	-2.5	nd
279	4	-22	1	-4.1	0.16	387	1	-19	nd	-3.5	nd
272	3	-22	1.7	-4.2	0.02	389	1	-21	nd	-3.6	nd
280	2	-21	nd	-4.2	nd	395	2	-21	nd	-3.9	nd
281	3	-25	1.2	-4.5	0.08	396	1	-21	nd	-3.8	nd
319	2	-16	nd	-3.2	nd	398	1	-20	nd	-3.6	nd
320	6	-20	4.03	-4.0	0.47	**Total**	**85**	**-21**	**2.9**	**-3.9**	**0.45**
321	2	-23	nd	-4.2	nd	Min		-29		-5.3	
322	2	-17	nd	-3.5	nd	Max		-9		-2.5	
323	2	-21	nd	-3.9	nd						
Grand Total	**115**	**-21**	**2.91**	**-3.9**	**0.48**						
Min		-29		-5.3							
Max		-9		-2.5							

4.1.3 Monthly-integrated drip water isotope sampling 2011-2013

Following on from the 2010-2011 spot sampling, monthly-integrated drip water isotope sampling began in 2011, and continued until 2013 (Figure 2). The results from site 3 were reported in Cuthbert et al. (2014a) and are shown on Figures 2 and 3. Here, we report results for site 1 in Figures 2 and 3 and in Table 4. Linear regression for the total monthly-integrated drip water samples at both site 1 ($r^2 = 0.77$) and site 3 ($r^2 = 0.81$) (Figure 3B) show that site 1 drip waters have a lower slope (5.9) than site 3 (7.1) and both are below the average slope of 8 for meteoric precipitation waters. A Mann-Whitney U test confirmed that the samples from these two sites were significantly different with respect to $\delta^{18}O$ ($\rho = 0.025$, $\alpha = 0.05$). The slopes of drip waters from individual drips at site 1 also varied considerably, with a range of 3.4 to 7.0 (Table 4).

Table 4. Site 1 monthly-integrated drip water sampling results, including: number of samples (n), mean δD composition (μ δD**),** standard deviation relative to previous column (SD), mean $\delta^{18}O$ composition (μ $\delta^{18}O$), slope (M), error term (C) and regression coefficient (r^2).

Linear Regression: $\delta D = M*\delta^{18}O + C$

site ID	n	μ δD	SD	μ $\delta^{18}O$	SD	M	C	r^2
326	11	-12	4.3	-2.9	0.61	4.2	-0.1	0.35
331	5	-3	9.3	-1.4	1.39	6.7	6.5	0.98
361	15	-10	4.9	-2.3	0.95	3.4	-2.2	0.45
364	13	-8	8.4	-2.3	1.16	6.2	6.3	0.75
385	12	-3	9.5	-1.5	1.30	7.0	7.3	0.91

Comparing all of our isotopic data in Figures 3A and 3B show differences between datasets. The spot sampling data cluster at the lower range of the monthly-integrated values (Figure 3A). The two sample populations are statistically different for both $\delta^{18}O$ and δD using a Mann-Whitney U test ($\rho = <0.0001$, $\alpha = 0.05$), revealing a bias of depleted isotopic composition from spot samples compared to monthly averaged

values. Although the spot and monthly-integrated samples were collected during different time periods we interpret that the difference is due to experimental bias rather than representative of different mean isotopic composition. For example, it may be biased to samples with sufficiently high drip rates to collect enough water (i.e. 28 ml to fill a sample vial) and thus potentially bias isotopic drip water results, in the same way that is known to occur with drip rate (i.e. Markowska et al., 2015; Mariethoz et al., 2012).

Monthly-integrated drips from site 3 generally showed a similar trend in $\delta^{18}O$ over time, i.e. depleted values and a lower range in March 2011 (-3.3‰ to -4.2‰) and more enriched values and a larger range in November 2011 (-0.0‰ to -3.4‰) (Figure 2). This does not appear to be a seasonal trend, as cycles of enrichment and depletion do not consistently occur during specific months of the year, rather periods of depletion occur after months were P>PET, and there is potentially a few months lag time. For example, P>PET in October 2011, which started a downwards trend towards depleted $\delta^{18}O$ with a lag of 2 months and the trend continued further after February and March 2012 where P>PET. Site 1, however, did not show this trend as clearly (Figure 2). Following a prolonged drip discharge response, the range in drip water isotopic composition was lower and on most occasions clustered around the monthly rainfall isotopic composition over the same time period. For example, March 2012 (Figure 2), where P was approximately double PET, therefore suggesting a high potential for infiltration of rainfall.

4.2 Irrigation experiment 2013

The sites that were activated, following the 2013 irrigation experiment, are shown on the map in Figure 1 and summarised in Table 1. The $\delta^{18}O$ and δD data over the whole

irrigation as well as pre-irrigation baseline data are shown in Figure 4 and a time series are shown in Figure 5. No discharge occurred at sites 1 or 2 prior to the artificial irrigations (i.e. all drip sites were dry); therefore we interpret that drip response was directly related to the irrigations. Irrigation 1 only activated drips WS9 and WS10 at site 2, producing drip water that was between ~7 and -12 δD (Figure 5) and clustered with pre-irrigation drip data (Figure 4). On subsequent irrigations (2-4) discharge was also activated at drips WS1, WS2, WS16 and WS21 at site 1 and drip WS11 at site 2, however no discharge response was ever observed at site 3. We examine the response of each drip in detail below in sections 4.2.1 for site 1 and 4.2.2 for site 2. Drips were sampled again, 6, 10 and 12 months after the irrigation experiment and the results are presented in section 4.2.3.

4.2.1 Site 1 drip responses

WS1 and WS2 activated after the irrigation 2, approximately 2.5 hours after irrigating began. Both sites exhibited a hydrograph response to infiltration, with a very sharp initial peak, followed by an exponential recession before ceasing 3 hours and 45 minutes later (Figure 5). WS1 had higher discharge volumes with a maximum rate of 165 drips per minute, versus 59 drips per minute at WS2 (Figure 5). There was a small increase in drip water δD at WS1 over the first hydrograph from -18‰ to -9‰ (Figure 5) and could indicate early tracer arrival. However, the isotopic compositions of all drip waters after irrigation 2 were within the isotopic range of pre-irrigation data (Figure 4), suggesting that no tracer was present in these initial drip waters. They were also different from the isotopic composition of water from irrigation 2 (Figure 4), which was similar to precipitation-weighed mean annual rainfall, therefore we

suggest this was pre-existing storage water in the unsaturated zone, expelled as a direct result of irrigation (e.g. via piston-flow, Tooth and Fairchild, 2003).

Irrigation 3 activated drips WS16 and WS21, however discharge volumes were low (i.e. WS21 10 mL over ~10 hours) short-lived hence no drip rate data appear on Figure 5 for these drips. Interestingly, drips WS16 and WS21 had the highest δD values observed in drip discharge waters over the whole 2013 irrigation experiment, suggesting they carried the highest concentration of tracer. Maximum δD concentrations for WS16 and WS21 were 108‰ and 245‰ respectively, suggesting an apparent dilution factor of 1.8% and 4.0%, respectively. In comparison, peak δD concentration also occurred at drips WS1 and at WS2 after irrigation 3 and was 12‰ and 9‰, respectively. This result suggests apparent dilution factors of 0.19% and 0.15% from initial concentration, respectively. This implies that water with higher concentrations of tracer activated later (after irrigation 3, not irrigation 2). Also, unlike previous irrigations 1 and 2, dripping continued at drips WS1 and WS2 until the start of the next as opposed to after irrigation 2, when dripping stopped several hours later.

Finally, following irrigation 4, WS1 and WS2 had the fastest discharge rates, peaking at 233 and 122 drips per minute, respectively, suggesting that antecedent soil moisture conditions must be of particular importance in controlling discharge response at site 1. Dripping ceased at WS1 approximately 28 hours later and at WS2 approximately 24 hours later and a final mixed sample was collected at both WS1 and WS2, representative of 16- and 12-hour period, respectively. Drips WS16 and WS21 ceased dripping after shortly after irrigation 4, however the exact timing is unknown due to an absence of drip logger data.

520 *4.2.2 2013 Site 2 drip responses*

521 During the irrigation experiment drip sites WS9, WS10 and WS11 were activated.
522 Unlike site 1, drip responses at site 2 activated during irrigation 1 but drip rates were
523 much lower overall (Figure 5). Drips WS9 and WS10 activated approximately 14
524 hours later at a rate of approximately 1 and 3 drips per minute, respectively, which
525 slowly decreased over the following 6 days to approximately 1 and 2 drips per
526 minute, respectively. We suggest a possible reason that drips activated at site 2 but
527 not site 1 during irrigation 1 was due to the small difference in the irrigation patch
528 area, which was moved closer to site 1 on subsequent days. Alternatively, as the 35
529 mm irrigation did not meet the minimum 60 mm rainfall observed in Jex et al. (2012)
530 to initiate a drip discharge response, there may not have been sufficient water
531 irrigated to result in cave discharge.

532 Compared to site 1, flow at site 2 remained relatively constant over the entire
533 irrigation experiment. After irrigation 4, drip WS11 activated for the first time, but
534 had a very slow drip rate and was only sampled once, three days after irrigation 4,
535 resulting in a mixed sample of the previous three days (Figure 5). Importantly, no drip
536 waters collected at site 2 showed any evidence of deuterium tracer present (Figure 4,
537 5). We suggest discharge was initiated by a piston effect, or pressure effect from the
538 irrigation water pressurising deeper stores within the epikarst. Drip water samples
539 grouped around the LMWL (Figure 4), and showed low intra-site, but large inter-site
540 isotopic variability with approximately 20‰ differences with respect to δD. This
541 suggests that pre-existing older storage water was discharged from drips at site, which
542 originated from discrete stores, which contained waters with very different isotopic
543 composition. It would be interpreted that these were from near-surface epikarst stores

owing to their enriched isotopic composition in relation to precipitation-weighted mean annual rainfall and that they sit close to the LMWL (Figure 4); suggesting that do not come from highly evaporated soil stores associated with low slope values (<6) (Barnes and Allison, 1988).

4.2.3 2013-14 Post irrigation sampling

Three campaigns to collect post irrigation drip waters were conducted 6, 10 and 12 months later, to investigate whether deuterium tracer was still present in the drip waters. Drip samples were opportunistically collected from active drips at sites 1, 2 and 3 (Figure 1) and the results can be seen in Figure 6, compared with pre-irrigation data. The post-irrigation were not statistically different from monthly-integrated samples using a Mann-Whitney comparison (p-value = 0.661, 0.347 and 0.399 for 6 months, 10 months and 12 months respectively, α = 0.025). Thus, this result suggests that the tracer was previously removed from the drip site flow paths (i.e. due to processes such as evaportranspiration, lateral flow, or infiltration) prior to post irrigation sampling. We suggest that water residence times in 2013 were <6 months. However, this conclusion cannot be generalised for the whole cave system since residence times would also depend on antecedent conditions of rainfall and moisture content in the soil zone and may also spatially vary within the cave (i.e. at deeper site 3).

4.3 Irrigation experiment 2014

The second set of artificial irrigations conducted in Jan 2014, that included a 'wetting-up' period prior to the addition of deuterium tracer, are presented in Figures 7 and 8, as well as the evaporation pan data (Table 5). Before irrigating, no drip sites at site 1

were actively dripping and sampling was only attempted at site 1, as it was the only site to show evidence of tracer during the 2013 irrigation experiment. During irrigation 5 drips WS1 and WS2 activated as well as drips WS4 and WS6, which had not previously activated. During irrigation 6, drip WS16 activated and an additional two drips, WS25 and WS30, which had not previously activated.

4.3.1 2014 Site 1 drip responses

After irrigation 5, drips WS1, WS2 and WS4 activated approximately 3 hours after irrigating started and WS6 approximately 4 hours later (Figure 7). Water isotope samples from WS1 showed very low isotopic variability between samples (Figure 7). Deuterium tracer was added to the irrigation water during irrigation 6. Due to pre-wetting from the previous day, discharge responses were more immediate at all drips (~ 2 hours after irrigation commenced) and the peak tracer concentration was much earlier, approximately 5 hours after irrigating commenced, for drips WS1, WS2 and WS4. Additional drips also activated including WS16, WS25 and WS30 at approximately 11 hours, 3.5 hours and 3.75 hours later, respectively. Drips stopped approximately 28 hours after irrigation 7, which was exactly the same time as WS1 stopped dripping in the 2013 irrigation experiment. WS6 was the only drip to continue dripping after the experiment at 2-3 drips per minute.

The most significant feature of the 2014 irrigation experiment was a greater maximum concentration of deuterium tracer observed in drip waters (where the tracer was present) as opposed to the 2013 irrigation experiment. WS30 had the highest concentration of δD (640.4‰), indicating an apparent dilution factor of 9.6%, based on the original δD composition of irrigation water containing tracer (6700 δD). Other drips also had higher concentrations of deuterium tracer, for example: WS1 = 226‰

591 (apparent dilution factor of 3.37%), WS2 = 224‰ (apparent dilution factor of 3.35%)
592 and WS4 = 235‰ (apparent dilution factor of 3.50%).

593 However, not all sites showed such elevated concentration of δD, for example drips
594 WS16 and WS25, which only activated on the second day, after irrigation 7, had
595 maximum δD of 20.5‰ and 63.0‰, respectively, as the tracer may have been diluted
596 further by subsequent irrigating. The first drip water sample from WS16 is
597 comparable to pre-irrigation values (Figure 7), indicating that the initial water
598 discharged from this drip is likely to be storage water already present in the system.
599 Lastly, WS6, a very slow drip (1-9 drips per minute), did not show any deuterium
600 tracer (Figures 7, 8) and was also the only one to continue dripping days after the
601 experiment. Drips that did not respond to irrigation 5 also appear to have less tracer
602 present in discharge waters, apart from WS30 which activated after irrigation 7, and
603 also had the highest tracer concentration (Figure 8).

604 *4.2.2 2014 Post irrigation sampling*

605 One sampling campaign was conducted 6 months after the 2014 irrigation
606 experiment. Drip water samples were opportunistically collected from sites 1, 2 and 3
607 and the results are shown in Figure 9. Evidence of residual deuterium tracer was
608 observed at site 1 and site 2, but not site 3 (Figure 9). This contrasts with the results
609 from the 2013 post irrigation samples, which showed no tracer present at any site. At
610 site 1 the final δD samples taken at the end of the 2014 irrigation were between 20 –
611 90%. Six months later, the range of δD in drip water samples was -31 to +55‰,
612 strongly suggesting that irrigation waters from irrigation 6 were still present in the
613 vadose zone above site 1. WS6, which during the 2014 irrigation did not show any
614 measureable deuterium tracer in drip waters, showed evidence of tracer present in the

post irrigation drip water (Figure 9), indicating that this drip is fed by slow percolation from the irrigation area and also that there must be substantial storage in the unsaturated zone above this site. WS11 (site 2), 7 m away laterally from irrigation-activated drips at site 1, also showed evidence of the deuterium tracer, suggesting subsurface connectivity between site 1 and site 2.

4.3.3 Evaporation pan results

The results from six evaporation pans sites in CC and on the surface, monitored during the 2014 irrigation experiment, are shown in Table 5. The surface evaporation pan had a volumetric loss of 1.2 mm/d, which was associated with a total enrichment rate of ^{18}O and ^{2}H of +0.6‰/h and +1.9‰/h, respectively. In the cave we also observed volumetric loss of evaporation pan water (Table 5). Shallower sites closer to the entrance, for example 'entrance' and 'site 1' in Table 5, show a volumetric loss of 0.30 and 0.14 mm/d, respectively, which was associated with the same enrichment of ^{18}O of +0.2‰/h. At the deepest site in the cave we observed both the lowest volumetric loss of water (0.004 mm/d) as well as the lowest enrichment rate of ^{18}O and ^{2}H, +0.1‰/h and +0.4‰/h, respectively.

Table 5. Evaporation pan results for the land surface and five cave areas at different depths (0 m to -25 m) in shallowest to deepest.

Sites	Time (h)	$\delta^{18}O$	δD	Total Volumetric loss (mm/d)	Total Enrichment ($\delta^{18}O$)	Total Enrichment (δD)	Enrichment (p/h) ($\delta^{18}O$)	Enrichment (p/h) (δD)
Initial Concentration	0	-4.9	-26					
Surface	22	7.7	16	1.20	12.5	42	0.6	2
Entrance	21	-0.2	-3	0.30	4.7	23	0.2	1
Site 1	21	-1.5	-7	0.14	3.3	20	0.2	1
Site 2	21	-2.4	-13	0.11	2.5	13.	0.1	1
Mid-cave	21	-3.0	-12	0.09	1.8	15	0.2	1
Site 3	22	-3.4	-18	0.04	1.5	8	0.1	0.5

5. Discussion

We examined the various roles that factors such as karst hydrology, evaporation and antecedent pre-conditions had on the evolution of drip water isotopic composition. Here, we will firstly address the importance of 'wetting up' in controlling infiltration, the role of karst hydrology revealed from our irrigation experiments and then the importance of evaporation as a dominant control on the isotopic composition of drip waters from a semi-arid site. The implications for $\delta^{18}O$ interpretation in speleothem records are then evaluated.

5.1 Soil moisture deficit and the significance of 'wetting up'

The soil zone at CC generally has substantial soil moisture deficits due to high PET that reduce potential for infiltration of rainfall to the cave below. Soil moisture deficits have been previously highlighted by studies such as Oster et al. (2012), which showed that when large soil moisture deficits exist, the majority of rainfall is absorbed by the soil zone and does not infiltrate to the epikarst below. Over our pre-irrigation study period (2011-2014) there were 13 months, often during winter, where P>PET (Figure 2). As a consequence these periods often coincided with cave discharge responses at shallower site 1, but less frequently at site 3 (Figure 2). Thus, site 1 appears to be more responsive to surface infiltration, but requires a minimum amount of rainfall to be delivered to initiate discharge. Our irrigation experiments revealed that after irrigation 1, which delivered an equivalent 35 mm rainfall, no drips activated at site 1. In contrast, irrigation 5, which was approximately twice the equivalent rainfall (68 mm), was sufficient to surpass the minimum theoretical field capacity calculated by Rutlidge et al., (2014) and subsequently caused drip activation

via preferential flow paths. We suggest a minimum rainfall amount of ~60 mm is required to initiate recharge following a dry period, which is agreement with drip discharge observations from Jex et al. (2012). At Wellington, the annual mean days per year of rainfall >50 mm is 0.7, which suggests that there are likely to be 0-1 infiltration events per year. Often these intense rainstorms are associated with low $\delta^{18}O$ (Dansgaard, 1964; Rozanski et al., 1993; Gat, 1996; Clark and Fritz, 1997). However, for karst systems with evaporation in the unsaturated zone, this could be balanced by or exceeded by the amount of evaporative enrichment, which will be further discussed in section 5.3.

Drip discharge responses of approximately 0.7 per year are consistent with observations in pre-irrigation data from less responsive and more attenuated site 3, but not site 1, which showed more frequent discharge responses (i.e. 7-11 per year) (Figure 2). This could be attributed to the importance of 'pre-wetting', where once the soil zone has been 'primed' a much smaller rainfall event can result in a cave discharge response. For example, irrigation 6, which was only equivalent to a 20 mm rainfall event, resulted in cave discharge at site 1 drips (Figure 8).

The irrigation experiments also revealed information not only about the amount of infiltration required to initiate drip responses, but also information about how water may move and be distributed in the sub-surface. Concentration of tracer measured in drip waters from the 2014 irrigation experiment were approximately 3 times greater than in 2013 and several factors may have contributed to this. Firstly, the timing of tracer introduction in the first irrigation of the 2013 irrigation experiment compared to 2014, which incorporated a 'pre-wetting' irrigation, may have contributed to tracer loss. This could be due to capillary driven flow of deuteriated water into low-

permeable clay rich zones at early stages of the irrigation 1 when the soil was very dry. Water held in clay rich zones would be difficult to mobilise by subsequent irrigations due to low permeability and may have prevented tracer redistribution to the unsaturated zone below. This mechanism was observed in soil experiments by Greve et al. (2010; 2012). Secondly, dilution from subsequent irrigations (2 to 4) may have diluted the initial tracer concentration. Thirdly, dry antecedent conditions could have allowed more opportunity for lateral flow and evapotranspiration in the soil zone. In comparison, in 2014, irrigation 5 served to 'prime' the dry soil zone, thus allowing a fast response to the tracer irrigation 6, where tracer was observed in cave drip waters only hours later after its introduction (Figure 8).

5.2 Karst hydrological controls on isotopic composition

Despite irrigating directly over site 1, located <5 m below the surface, dripping at our pre-irrigation monitoring sites located directly underneath was rare. During the 2013 irrigations (1 to 4) none of the pre-irrigation drips were activated at sites 1 or 3. In the 2014 irrigations (5 to 7) only one pre-irrigation drip (361/WS6) activated at site 1, but showed no evidence of tracer during the experiment (Figure 7). This is despite the fact that pre-irrigation drips and irrigation-activated drips were spatially often only ~1 m apart (Figure 1). Our results highlight the importance of flow heterogeneity in karst systems. At CC site 1, subsurface flow to the pre-irrigation monitoring drips must originate from outside the surface irrigation area.

Our tracer experiments also identified highly variable water residence times within a relatively small spatial area. A feature of both irrigation experiments was a pulse of non-irrigation water, i.e. water of a different isotopic composition with no evidence of

tracer, being discharged to drips prior to infiltration water (Figures 4 and 7). This may suggest a piston-flow mechanism of flow delivery, with older storage water initially discharging from drips, similar to that observed in Fernandez-Cortes et al. (2008) in a semi-arid cave in Spain. At shallow site 1 (< 5 m), there was also evidence of tracer remaining 6 months after the 2014 irrigation experiment (drip 361/WS6; δD = 25‰, Figure 9) but not after the 2013 experiments (Figure 6). At the same time, tracer was also observed at deeper (-10 m) site 2 for the first time (Figure 9), demonstrating the importance of lateral flow. The latter may result from delayed diffusion of tracer from low permeable zones, for example clay-filled fractures in the epikarst. Evidence of attenuated residual tracer present 6 months later, demonstrates a minimum residence time in this shallow karst of at least 6 months. The reason why this was not observed in 2013 may be due to a combination of factors, (1) water from irrigation 1, including the tracer, was bound in clay rich soils and more difficult to mobilize and thus remained evaporating in the soil zone, (2) it had been previously discharged into the cave prior to the six month collection, and (3) it had undergone substantial dilution from subsequent three irrigations. Conversely, in 2014 as a wetting-up period was added, this may have allowed more preferential flow of water into subsurface storage reservoirs, thus we observed it 6 months later.

Variable residence times exist at CC that are highly dependent on the antecedent conditions, determining the available storage capacity in the soil as well as the karst fractures and stores, which may contain little or no water. In addition, we demonstrate a spatial heterogeneity of drip water responses to our irrigation experiments. Variable residence times and the heterogeneity of flow paths help explain the range in drip water isotope composition in the pre-irrigation data at a single point in time. For

example, in monthly sampling from November 2012 both sites 1 and 3 (Figure 2) have a range in isotopic composition between different drips for $\delta^{18}O$ of 3.16‰ and 3.3‰, respectively. This can be attributed to the karst hydrology, which permits unique flow paths and storage reservoirs, feeding individual drip sites with water that has undergone unique isotopic evolution. Our results can thus be extended to drip water isotopic composition in other semi-arid areas, which typically have infrequent rainfall recharge events, and the isotopic composition of associated speleothems.

5.3 Evaporative enrichment of $\delta^{18}O$ in drip waters

This study has shown that at shallow site 1, pre-irrigation data are relatively enriched by up to +21‰ (δD) and up to +2.9‰ ($\delta^{18}O$), compared to precipitated-weighted mean annual rainfall. This is similar to the isotopic enrichment previously observed in drip waters from site 3 in Cuthbert et al. (2014a), thus demonstrating that waters infiltrating two distinct areas of the cave with different flow paths, both experience subsurface evaporation. However, we show that this isotopic enrichment varies between sampling areas as sites 1 and 3 had statistically different δD and $\delta^{18}O$ datasets, and therefore the nature of evaporative enrichment at sites 1 and 3 may be different. At site 3, Cuthbert et al. (2014a) demonstrated that cave drip water had undergone evaporation in a high humidity environment (>95%), postulated to be a near-surface epikarst store. However, at site 1, we observe shallower slopes of the drip water regression lines (Table 4) and moderate correlation ($r^2 = 0.59$) between the regression correlation coefficients and the range of slope values (Table 3). This is indicative of non-equilibrium evaporative conditions at this shallow site. Significant slope variability between drips at site 1 is also observed (from 3.4 to 7.0; average 5.9), which is more consistent with local evaporation line values between 4 and 6 (Gibson

et al., 1993). The shallowest slope gradient (3.4) is observed at drip 361/WS6, which the tracer experiments demonstrated could contain water with a six-month residence time. Thus we suggest that evaporative enrichment at site 1 must occur in a less humid environment (i.e <95%) than that for site 3. This could be in a very shallow karst store or soil-filled fracture, that has a greater connectivity to the overlying soil compared to site 3, giving rise to the lower average slope of 5.9 (Figure 3B). It seems likely that the extent of drip water evaporative enrichment at this shallow site is limited by the water residence time.

In the section 5.2 we discussed the role of karst hydrology and variable water residence times on the evolution of drip water isotopic composition from the original composition of rainfall input. We demonstrated that these processes could explain the inter-drip variability of oxygen isotope composition. However, the most dominant control on drip water oxygen isotopes is subsurface evaporation, which determines both the offset from the precipitation-weighted mean annual rainfall, and the temporal trends in drip water isotopic composition (Figure 2). This leads to an enriched drip water isotopic composition.

5.4 Implications for $\delta^{18}O$ of speleothem proxy records

The $\delta^{18}O$ signal recorded in speleothems is a function of the isotopic composition of rainfall and any subsequent transformations between that source and the incorporation of oxygen into the speleothem calcite. Excluding kinetic fractionation processes which occur during the formation of calcite (Hendy, 1971; Mickler et al., 2004; Affek et al., 2014), subsequent transformations include: non-stationary and flow path variability (Arbel et al., 2010; Treble et al., 2013; Moerman et al., 2014; Williams,

2008), subsurface evaporation (Bar-Matthews et al. 1996; Ayalon et al. 1998), antecedent conditions (Sheffer et al., 2011; Markowska et al., 2015), residence times (Genty et al., 2014) and bias to high magnitude rainfall events (Treble et al., 2013; Moerman, et al., 2014). In semi-arid environments, the isotopic signature of drip waters and associated speleothems are likely to be controlled by different factors compared to tropical or temperate environments, due to their drier climatic conditions and more episodic infiltration.

5.4.1 Flow variability

The importance of understanding unsaturated zone water movement was highlighted in the two irrigation experiments performed in this study, which revealed the water feeding drips less than 1 m apart can undergo very different routing in the unsaturated zone, even at the most shallow cave chamber sites (~2 m overburden). This can lead to a large range in drip water isotopic composition at any one point in time, which at our site was up to 3.4‰ ($\delta^{18}O$). This may potentially lead to adjacent and coeval stalagmites producing different speleothem $\delta^{18}O$ records from a single climate forcing. Although previously observed (McDermott et al., 1999; Lachinet, 2009), we hypothesise that this variability will be greatest in semi-arid to arid zone speleothems. Here, soil and water storage capacity is likely to be high, due to dry antecedent conditions. This will produce greater heterogeneity of drip water, and associated speleothem isotopic composition, compared to temperate and tropical sites with greater water excess and a higher likelihood of mixing of waters of different age and flow path.

5.4.2 Speleothem $\delta^{18}O$ alteration from in-cave processes

798 The speleothem $\delta^{18}O$ signal may also be altered during calcite precipitation,
799 potentially resulting in isotopic disequilibrium or kinetic fractionation (Hendy, 1971).
800 In our monitoring, we limited the effects of in-cave evaporation of water through the
801 use of paraffin oil in sample containers. However, in semi-arid and arid zone caves
802 which have a relative humidity <100%, speleothem formation at slow drip rates
803 provides sufficient time for in-cave evaporative fractionation of drip waters to occur
804 during calcite precipitation (Dreybrodt and Scholz, 2011). From our evaporation pan
805 data, site 1 (with a lower and more variable relative humidity, median 88.6%, Rau et
806 al., 2015) demonstrated a significant ^{18}O-enrichment over a relatively short time
807 period (0.16‰/hr). In contrast, site 3 exhibited a higher relative humidity (97.1%, Rau
808 et al., 2015) and lower observed isotopic enrichment at (0.07‰/hr, Table 5). Also,
809 due to its lower humidity and near-entrance location, speleothem forming drip waters
810 at site 1 may also be subject to evaporative cooling demonstrated by Rau et al. (2015)
811 and Cuthbert et al. (2014b). We propose that the latter site would be one most suitable
812 for choosing speleothem samples for oxygen isotope analysis where within-cave
813 evaporative fractionation and evaporative cooling would be minimised. We note,
814 however, that drip water evaporative enrichment is likely still to have occurred (see
815 section 5.4.1). Also, the CC study site might be relatively unique for semi-arid and
816 arid zone karst areas in having a chamber with consistently high relative humidity,
817 due to the local water table being adjacent to the chamber, maintaining a supply of
818 water vapour.

819 *5.4.3 Evaporative enrichment*

820 The effect of evaporation in semi-arid karst can occur due to high surface
821 evaporation, creating water-limited environments associated with soil moisture

deficits. This can create environments for subsurface evaporation of storage water to occur as well as the in-cave processes discussed previously (section 5.4.2). We have demonstrated that drip water is ^{18}O-enriched due to evaporation of storage water in the soil and karst. This suggests that the interpretation of speleothem $\delta^{18}O$ from semi-arid environments should be as a combined signal of (1) evaporative enrichment in the subsurface and (2) the initial input composition of the rainfall, as well as any within-cave isotope fractionation process.

Speleothem deposition may be seasonally biased, especially in caves which ventilate seasonally and have the lowest cave air carbon dioxide in winter (James et al., 2015). Speleothem deposition may be more likely or more rapid during winter months, which in semi-arid regions is the season of lowest PET (Figure 2). Therefore, it might be expected that the effects of evaporative enrichment may be countered to some extent by a bias to winter deposition. Grey bars on Figure 2 indicate when drip waters are most likely to contribute to speleothem growth at CC, and hence the speleothem record, based on differences of outside versus inside cave temperature from Rau et al. (2014). However, at CC, because subsurface evaporation occurs over many months, drip waters were also ^{18}O-enriched during the winter months (Figure 2). Speleothem oxygen isotope records may therefore preserve the evaporative enrichment signal to varying degrees, depending on the extent of seasonal ventilation of the cave, and the amount and duration of subsurface evaporative enrichment.

5.4.4. Bias towards high-magnitude, winter season, rainfall events

The effect of high daily evapotranspiration in semi-arid regions means that the $\delta^{18}O$ of recharge water is likely to be biased towards larger rainfall events that are able to

overcome soil moisture deficits. These rainfall recharge events may have an isotopic composition that is distinctive from the weighted mean of precipitation. At our site, events less than 60 mm are unlikely to be contribute to drip water at site 3 unless there has been wet antecedent conditions. This is less than other reported semi-arid zone studies, such as Sheffer et al., (2011), that stated a minimum of 100 mm and we attribute this difference to the shallow soil (~0.3 m) above CC. We also do not observe winter seasonal dominance in rainfall, as reported by other studies in semi-arid environments (Cruz-San Julian et al., 1992; Bar Matthews et al., 1996). However, with highest evaporation during summer months (Figure 2), we would expect a long-term bias towards greater recharge during winter months (when P>PET). At semi-arid karst locations where the speleothem oxygen isotopic composition was not dominated by evaporative processes, one would therefore expect them to contain a record of rainfall isotopic composition that is biased to the winter season and high magnitude events.

5.4.5 Summary

In semi-arid karst regions, the effects of all these processes affecting drip water oxygen isotopic composition need to be constrained at the individual drip site, prior to any speleothem interpretation. Dorale and Liu (2009) discuss the importance of vadose zone and kinetic processes in overprinting the isotopic signals in speleothems, ultimately masking the primary environmental signal, and suggest the Replication Test as a robust method to test for the absence of kinetic and vadose zone processes. Ultimately in speleothems from CC, and probably most semi-arid regions where prior evaporation of drip waters occurs, the primary signal will be that of evaporative processes (either subsurface or within-cave), which occur subsequent to any

infrequent rainfall recharge events. Speleothem oxygen isotope records should be expected to be out of isotope equilibrium, but the 'environmental signal' contained within them is one which can be quantified as a proxy for the frequency of rainfall recharge (more frequent recharge events = less evaporated drip waters). However, the 'replication test' would have to be redefined to permit a greater variability between speleothems and to recognise the replicated record is one that includes non-equilibrium processes.

State-of-the-art sampling techniques now available using micro-mill drilling at <0.1 mm increments, as little as 50 micro grams of speleothem sample is required for IRMS (Isotope Ratio Mass-Spectrometry) carbonate $\delta^{18}O$ analysis. For slower growing stalagmites, often associated with semi-arid environments, SIMS technology (i.e. Orland et al. 2014) allows speleothems to be sampled at approximately monthly resolution, enabling highly resolved records of paleo-aridity/recharge from speleothems from semi-arid caves. As the main driver of Australian rainfall variability, particularly eastern Australia, is the El Nino Southern Oscillation (ENSO) (Risbey et al., 2009), wet and dry periods at CC are likely to relate to variations in the Southern Oscillation Index (SOI). Multi-year periods of decreased rainfall, and increased time in-between infiltration events are likely to result in enrichment of stored cave drip waters. Thus, speleothems from CC have the potential to record ENSO variability at this particularly sensitive site.

6. Conclusion

This study emphasises several key factors that are relevant to karst hydrology in semi-arid environments and the subsequent impacts this may have on speleothem-derived

892 $\delta^{18}O$ paleoclimate records. Evaporative processes dominate the hydrological balance
893 in water-limited regions where recharge events are episodic and infrequent. In the
894 subsurface, we demonstrate that evaporation dominates the $\delta^{18}O$ composition of drip
895 waters, which are enriched relative to the precipitation-weighted mean annual rainfall
896 isotopic composition. We used a conservative deuterium tracer to reveal the flow path
897 variability and mixing fractions. This demonstates that variability is large even for
898 shallow drips (<5 m below the surface) that are only <1 m apart. Different flow
899 routing in the unsaturated zone led to drip water $\delta^{18}O$ variability on monthly spatial
900 scales (up to ~3.5‰); however, on larger annual spatial scales, karst evaporation
901 punctuated by recharge events dominates the variability in isotopic drip water
902 composition. Large variability in flow routing is increased by dry antecedent
903 conditions and in semi-arid regions may result in weaker replication of speleothem
904 $\delta^{18}O$ records. Semi-arid zone speleothem $\delta^{18}O$ archives, are more likely to record
905 recharge frequency not rainfall composition.

906 ## Acknowledgements

907 We thank the staff at Wellington Caves for their support. Funding for this research
908 was provided by the ARC DP110102124, and the National Centre for Groundwater
909 Research and Training, an Australian Government initiative, supported by the
910 Australian Research Council and the National Water Commission. Mark Cuthbert was
911 supported by Marie Curie Research Fellowship funding from the European
912 Community's Seventh Framework Programme [FP7/2007-2013] under grant
913 agreement no. 299091.We would like to further thank Barbora Gallagher and Scott
914 Allchin for their assistance with running stable isotope sampling on the ANSTO
915 Picarro instrument. We thank Bruce Welsh and Philip Maynard from Sydney

University Speleological Society for the cave survey map template that we modified. Ashley Martin is thanked for helpful discussions with the preparation of the manuscript. Finally, thank-you to the two anonymous reviewers and Colin Murray-Wallace for their detailed and extremely helpful comments, which have greatly improved this manuscript.

References

Affek, H.P., Matthews, A., Ayalon, A., Bar-Matthews, M., Burstyn, Y., Zaarur, S., Zilberman, T. 2014. Accounting for kinetic isotope effects in Soreq Cave (Israel) speleothems, *Geochimica et Cosmochimica Acta, 143, 303-318.*

Agnew, C., & Anderson, W. 1992. *Water in the arid realm*. Routledge: London.

Allison, G.B., and Hughes, M.W. 1983. The use of natural tracers as indicators of soil-water movement in a temperate semi-arid region. *Journal of Hydrology*. 60, 157-173.

Aquilina, L., Ladouche, B., and Doerfliger, N.2006. Water storage and transfer in the epikarst of karstic systems during high flow periods. *Journal of Hydrology*, 327, 472–485.

Aquilina, L., Ladouche, B., Dörfliger, N., 2005. Recharge processes in karstic systems investigated through the correlation of chemical and isotopic composition of rain and spring-waters. *Applied Geochemistry*, 20 (12), 2189–2206.

Arbel, Y., Greenbaum, N., Lange, J.,Inbar, M. 2010. Infiltration processes and flow rates in developed karst vadose zone using tracers in cave drips, *Earth Surface Processes and Landforms*, 35(14), 1682-1693.

Ayalon, A., Bar-Matthews, M., and Sass, E. 1998. Rainfall-recharge relationships within a karstic terrain in the Eastern Mediterranean semi-arid region, Israel: $\delta^{18}O$ and δD characteristics, *Journal of Hydrology*. 207, 18–31, doi:10.1016/s0022-1694(98)00119-x.

Baker, A., Barnes, W.L. and Smart, P.L., 1997. Stalagmite Drip Discharge and Organic Matter Fluxes in Lower Cave, Bristol. *Hydrological Processes*, 11, 1541-1555.

Baker, A. & Brunsdon, C., 2003. Non-linearities in drip water hydrology: an example from Stump Cross Caverns, Yorkshire. *Journal of Hydrology*, 277, 151-163.

Baker, A. Hellstrom, J.C., Kelly, B.F.J., Mariethoz, G., Trouet, V. 2015. A composite annual-resolution stalagmite record of North Atlantic climate over the last three millennia. *Scientific Reports* 5, 10307; doi: 10.1038/srep10307.

Baldini, J, McDermott, F, Hoffmann, D, Richards, D & Clipson, N 2008, 'Very high-frequency and seasonal cave atmosphere PCO_2 variability: Implications for stalagmite growth and oxygen isotope-based paleoclimate records'. *Earth and Planetary Science Letters*, vol 272 ., pp. 118 - 129

Bar-Matthews, M., Ayalon, A., Matthews, A., Sass, E., Halicz, L., 1996. Carbon and oxygen isotope study of the active water-carbonate system in a karstic Mediterranean cave: implications for paleoclimate research in semiarid regions. *Geochimica et Cosmochimica Acta* 60, 337-347.

952 Bar-Matthews, M., Ayalon, A., Kaufman, A., Wasserburg, G.J. 1999. The Eastern Mediterranean
953 paleoclimate as a reflection of regional events: Soreq cave, Israel, *Earth and Planetary Science Letters*,
954 166(1–2), 85-95.

955 Barnes, C.J., Allison, G.B. 1988. Tracing of water movement in the unsaturated zone using stable
956 isotopes of hydrogen and oxygen, *Journal of Hydrology*, 100, 143-176.

957 (BOM) Bureau of Meteorology. 2014. Climate statistics for Australian locations. *Bureau of*
958 *Meterology*, Melbourne, Australia [Accessed 21/10/2014]
959 http://www.bom.gov.au/climate/averages/tables/cw_065034.shtml

960 Burns, S. J., D. Fleitmann, M. Mudelsee, U. Neff, A. Matter, and A. Mangini. 2002. A 780-year
961 annually resolved record of Indian Ocean monsoon precipitation from a speleothem from south Oman,
962 Journal of Geophysical Research, 107(D20), 4434, doi:10.1029/2001JD001281.

963 Clark I. and Fritz P. 1997. *Environmental Isotopes in Hydrogeology*. Lewis Publishers. New York,
964 Boca Raton: p 328 .

965 Clemens, T., Huckinghaus, D., Liedl, R., Sauter, M., 1999. Simulation of the development of karst
966 aquifers: role of the epikarst. *International Journal of Earth Sciences* 88, 157–162.

967 Collister, C., & Mattey, D. 2008. Controls on water drop volume at speleothem drip sites: An
968 experimental study. *Journal of Hydrology*, 358(3), 259-267.

969 Craig, H., (1961). Isotopic variations in meteoric waters. *Science*, **133**: 1702-1703.

970 Cruz Jr., F. W., Karmanna, I., Viana Jr., O., Burnsb, S.J., Saild, A.N., Moreirae, M.Z. 2005. Stable
971 isotope study of cave percolation waters in subtropical Brazil: Implications for paleoclimate inferences
972 from speleothems. Chemical Geology, 3-4: 245-262.

973 Cruz, F.W. Jr., Burns, S.J., Karmann, I., Sharp, W.D., Vuille, M., Cardoso, A.O., Ferrari, J.A., Dias,
974 P.L.S. and Viana, O. Jr., 2005: Insolation- driven changes in atmospheric circulation over the past
975 116,000 years in subtropical Brazil, *Nature*, 434: 63-66.

976 Cruz San Julian JJ, Araguas L, Rozanski K, Benavente J, Cardenal J, Hidalgo MC, Garc´ıa Lo´pez S,
977 Martinez Garrido JC, Moral F, Olias M (1992) Sources of precipitation over South-Eastern Spain and
978 groundwater recharge. An isotopic study. *Tellus* 44B:226–236.

979 Cuthbert, M. O. & Tindimugaya, C. 2010. The importance of preferential flow in controlling
980 groundwater recharge in tropical Africa and implications for modelling the impact of climate change
981 on groundwater resources. *Journal of Water and Climate Cha nge*, 1, 234-245.

982 Cuthbert, M. O**.**, Mackay, R. & Nimmo, J. R. 2013. Linking soil moisture balance and source-
983 responsive models to estimate diffuse and preferential components of groundwater recharge. *Hydrol.*
984 *Earth Syst. Sci*., 17, 1003–1019.

985 Cuthbert (a), M. O., Baker, A., Jex, C. N., Graham, P. W., Treble, P. C., Andersen, M. S., & Ian
986 Acworth, R. 2014a. Drip water isotopes in semi-arid karst: implications for speleothem
987 paleoclimatology. *Earth and Planetary Science Letters*, 395, 194-204.

988 Cuthbert (b), M. O., Rau, G. C., Andersen, M. S., Roshan, H., Rutlidge, H., Marjo, C. E., Markowska,
989 M., Jex, C.N., Graham, P.W., Mariethoz, G. Acworth, R. I. & Baker, A. 2014b. Evaporative cooling of
990 speleothem drip water. *Scientific Reports*, 4.

991 Dansgaard, W. 1964. Stable isotopes in precipitation.*Tellu*s, 16(4) 436-468.

992 de Vries, J.J., Simmers, I., 2002. Groundwater recharge: an overview of processes and challenges,
993 Hydrogeology Journal, 10, 5-10.

994 Denniston, R.F., Wyrwoll, K., Asmerom, Y., Polyak, V.J., Humphreys, W.F., Cugley, J., Woods, D.,
995 LaPointe, Z., Peota, J., Greaves, E. 2013. North Atlantic forcing of millennial-scale Indo-Australian
996 monsoon dynamics during the Last Glacial period, *Quaternary Science Reviews*, 72, 159-168.

997 Dorale, J. A. and Liu, Z.H. 2009. Limitations of hendy test criteria in judging the paleoclimatic
998 suitability of speleothems and the need for replication, *Journal of Cave Karst Studies*, 71, 73–80.

999 Dreybrodt, W., & Scholz, D. 2011. Climatic dependence of stable carbon and oxygen isotope signals
1000 recorded in speleothems: from soil water to speleothem calcite. *Geochimica et Cosmochimica Acta*,
1001 75(3), 734-752.

1002 Fairchild, I. J., Baker, A. 2012. *Speleothem Science. From Process to Past Environment*. Wiley-
1003 Blackwell, Chichester, UK.

1004 Fernandez-Cortes, A., Calaforra, J.M., Sanchez-Martos, F. 2008. Hydrogeochemical processes as
1005 environmental indicators in drip water: Study of the Cueva del Agua (Southern Spain), International
1006 Journal of Speleology, 37(1), 41-52.

1007 Florea, L.J, Vacher, H.L. 2006. Springflow Hydrographs: Eogenetic vs. Telogenetic Karst.
1008 *Groundwater*, 44(3), 352-361.

1009 Ford, D.C. and P.W. Williams. 2007. *Karst geomorphology and hydrology*. 2nd ed. John Wiley &
1010 Sons, Chichester, U.K.

1011 Freeze, A.R., Cherry J.A. 1979. *Groundwater*. Prentice Hall Inc. NJ, USA.

1012 Fuller, L., Baker, A., Fairchild, I.J., Spötl, C., Marca-Bell, A., Rowe, P. and Dennis, P.F. 2008. Isotope
1013 hydrology of dripwaters in a Scottish cave and implications for stalagmite palaeoclimate research.
1014 *Hydrology and Earth System Sciences Discussions*, 5, 547-577.

1015 Gat,J.R. 1996. Oxygen and hydrogen isotopes in the hydrologic cycle: *Annual Review of Earth and*
1016 *Planetary Science*, 24: 225-262.

1017 D. Genty, I. Labuhn, G. Hoffmann, P.A. Danis, O. Mestre, F. Bourges, K. Wainer, M. Massault, S.
1018 Van Exter, E. Régnier, Ph. Orengo, S. Falourd, B. Minster. 2014. Rainfall and cave water isotopic
1019 relationships in two South-France sites, *Geochimica et Cosmochimica Acta*, 131, 323-343.

1020 Gibson, J.J., Edwards, T.W.D., Bursey, G.G., and Prowse, T.D., 1993. Estimating evaporation using
1021 stable isotopes: quantitative results and sensitivity analysis for two catchments in northern Canada,
1022 *Nordic Hydrology*, 24, pp. 79-94.

1023 Gibson, J.J. Birks, S.J., Edwards, T.W.D., 2008. Global prediction of δ_A and δ_2H-δ^{18}O evaporation
1024 slopes for lakes and soil water accounting for seasonality. Global Biogeochemical Cycles, 22, GB2031,
1025 doi:10.1029/2007GB002997.

1026 Gonfiantini,R.,1986. *Environmental isotopes in lake studies*, In:Fritz, P.,Fontes, J. Ch. (Eds.),
1027 Handbook of Environmental Isotope Geochemistry, vol.2: The Terrestrial Environment. Elsevier,
1028 pp.113–168.

1029 Greve, A., Andersen, M.S., Acworth, I. 2010. Investigations of soil cracking and preferential flow in a
1030 weighing lysimeter filled with cracking clay soil. Journal of Hydrology. 393: 105-113.

1031 Greve, A., Andersen, M.S., Acworth, I. 2012. Monitoring the transition from preferential to matrix
1032 flow in cracking clay soil through changes in electrical anisotropy. Geoderma. 179-180:46-52.

1033 Gunn, J. 1974. A model of the karst percolation system of Waterfall Swailet, Derbyshire. *Trans. British*
1034 *Cave Research Association.* 1 (3), 159-164.

Healy, R.W. 2010. *Estimating groundwater recharge*. Cambridge University Press, Cambridge, UK.

Henderson, G.M., 2006. Caving in to new chronologies. *Science* 313, 620–622.

Hendy, C.H.1971. The isotopic geochemistry of speleothems—I. The calculation of the effects of different modes of formation on the isotopic composition of speleothems and their applicability as palaeoclimatic indicators, *Geochemica et Cosmochimica Acta*, 35(8), 801-824.

Jex, C. N., Mariethoz, G., Baker, A., Graham, P., Andersen, M. S., Acworth, I., Edwards, N. & Azcurra, C. 2012. Spatially dense drip hydrological monitoring and infiltration behaviour at the Wellington Caves, South East Australia. *International Journal of Speleology*, 41(2), 14.

Jones, W.K. 2006. Physical structure of the epikarst. *Acta Carsologica*, 42(2-3):311-314.

Jones, I. C., and Banner, J. L., 2003, Hydrogeologic and climatic influences on spatial and interannual variations of recharge to a tropical karst island aquifer. Water Resources Research, 39(9): SBH51-SBH510.

Kaufman, A., Bar-Matthews, M., Ayalon, A., and Carmi, I. 2003. The vadose flow above Soreq Cave, Israel: a tritium study of the cave waters, *Journal of Hydrology*, 273, 155–163, doi:10.1016/s0022- 1694(02)00394-3.

Klimchouk A.B., 2004 - *Towards defining, delimiting and classifying epikarst: its origin, processes and variants of geomorphic evolution*. In: Jones, W.K., Culver, D.C. & Herman, J.S. (Eds.) – Epikarst. Special Publication 9. Charles Town, WV: Karst Waters Institute: 23-35.

Koeniger, P., Leibundgut, C., Link T., Marshall, J.D. 2010. Stable isotopes as water tracers in column and field studies. *Organic Geochemistry*. 41(1), 31-40.

Kuleshov, Y. 2012. *Thunderstorm and Lightning Climatology of Australia, Modern Climatology*, Dr Shih-Yu Wang (Ed.), ISBN: 978-953-51-0095-9, InTech, Available from: http://www.intechopen.com/books/modern-climatology/thunderstorm-and-lightning-climatology-of-australia

Labat, D.,Ababou, R., Mangin, A., 2000. Rainfall-runoff relations for karstic springs. Part I: convolution and spectral analysis. *Journal of Hydrology*, 238, 123–148.

Labat, D., Mangin, A., Ababou, R., 2002. Rainfall-runoff relations for karstic springs: multifractal analysis. *Journal of Hydrology*. 256, 176–195.

Landsberg, H.E. and Schloemer, R.W. 1967. *World Climatic Regions in Relation to Irrigation*. In Hagan, R.M., Haise, H.R., Edminster, T.W. (eds.), Irrigation of Agricultural Lands. American Society of Agronomy, Madison, USA.

Lachniet, M. S. 2009. Climatic and environmental controls on speleothem oxygen-isotope values, *Quaternary Science Reviews*, 28, 412–432.

Lou, W., Wang, S., Zeng, G., Zhu, X., Liu, W. 2014.Daily response of drip water isotopes to precipitation in Liangfeng Cave, Guizhou Province, SW China. *Quaternary International*, 349: 153-158.

McDermott, F., Frisia, S., Huang, Y., Longinelli, A., Spiro, B., Heaton, T. H., Hawkesworth C.J., Borsato, A., Keppens, E., Fairchild I.J., van der Borg, K., Verheydan, S., Selmo, E. 1999. Holocene climate variability in Europe: Holocene climate variability in Europe: Evidence from $\delta^{18}O$, textural and extension-rate variations in three speleothems. *Quaternary Science Reviews*, 18(8), 1021-1038.

McKnight TL, Hess D (2000) *Climate zones and types: dry climates (Zone B), physical geography: a landscape appreciation*. Prentice Hall, Upper Saddle River, NJ, pp 212–219

Mariethoz, G., Baker, A., Sivakumar, B., Hartland, A., & Graham, P. 2012. Chaos and irregularity in karst percolation. *Geophysical Research Letters*, 39(23) L23305, doi:10.1029/2012GL054270.

Markowska, M., Baker, A., Treble, P.C., Andersen, M.S., Hankin, S., Jex, C.N., Tadros, C.V., Roach, R. 2015. Unsaturated zone hydrology and cave drip discharge water response: Implications for speleothem palaeoclimate record variability. *Journal of Hydrology*, 529 part 2, 662-675.

Mickler, P.J., Banner, J.L., Stern, L., Asmerom, Y., Edwards, R.L., and Ito, E., 2004, Stable isotope variations in modern tropical speleothems: Evaluating applications to paleoenvironmental reconstructions: *Geochimica et Cosmochimica Acta*, 68, 4381–4393.

Moerman, J. W., K. M. Cobb, J. W. Partin, A. N. Meckler, S. A. Carolin, J. F. Adkins, S. Lejau, J. Malang, B. Clark, and A. A. Tuen (2014), Transformation of ENSO-related rainwater to dripwater δ18O variability by vadose water mixing, *Geophysical Research Letters*, 41, doi:10.1002/2014GL061696.

Onac, B.P., Sumrall, J., Mylroie, J.E. & Kearns, J. 2008. Cave minerals of San Salvador Island, Bahamas. *The University of South Florida Karst Studies Serie*s, 1, 68 p.

Orland, I.J., Burstyn, Y., Bar-Matthews, M., Kozdon, R., Ayalon, A., Matthews, A., Valley, J.W. 2014. Seasonal climate signals (1990–2008) in a modern Soreq Cave stalagmite as revealed by high-resolution geochemical analysis, *Chemical Geology*, 363, 322-333.

Osborne, R.A.L. 2007. Cathedral Cave, Wellington Caves, New South Wales, Australia. A multiphase non-fluvial cave. *Earth Surface Processes and Landforms*. 32: 2075-2103.

Oster, J.L, Montañez, I.P., Kelley, N.P. 2012. Response of a modern cave system to large seasonal precipitation variability, *Geochimica et Cosmochimica Acta*, 91, 92-108.

Pape, J.R., Banner, J.L., Mack, L.E., Musgrove, M., and Guilfoyle, A. 2010 Controls on oxygen isotope variability in precipitation and cave drip waters, central Texas, USA. *Journal of Hydrology*. 385, 203-215.

Perrin, J., Jeannin, P.-Y., and Zwahlen, F. 2003. Epikarst storage in a karst aquifer: a conceptual model based on isotopic data, Milandre test site, Switzerland. *Journal of hydrology*, 279, 106–124.

Rau, G.C., Cuthbert, M.O., Andersen, M.S., Baker, A., Rutlidge, H., Markowska, M., Roshan, H., Marjo, C.E., Graham, P.W., Acworth R.I. 2015. Controls on cave drip water temperature and implications for speleothem-based paleoclimate reconstructions. Quaternary Science Reviews. doi:10.1016/j.quascirev.2015.03.026

Risbey, J. S., Pook, M.J., McIntosh, P.C., Wheeler, M.C., Hendon, H.H 2009. On the remote drivers of rainfall variability in Australia. *Mon. Wea. Rev.* **137** (10), 3233-3253.

Rozanski, K., Araguas-Araguas, L. and Gonfiantini, R. (1993) Isotopic patterns in modern global precipitation: In: Climate Change in Continental Isotopic Records, P.K. Swart, K.C. Lohmann, J. McKenzie, and S.Savin, editors, *Geophysical Monograph* 78, American Geophysical Union, 1-36.

Rutlidge, H., Baker, A., Marjo, C. E., Andersen, M. S., Graham, P. W., Cuthbert, M. O., Rau, G. C., Roshan,H., Markowska, M., Mariethoz, G., Jex, C. 2014. Dripwater organic matter and trace element geochemistry in a semi-arid karst environment: Implications for speleothem paleoclimatology. *Geochimica et Cosmochimica Acta*, 135, 217-230.

Rutlidge, H. Andersen, M.S., Baker, A., Chinu, K.J. Cuthbert, M.O., Catherine Jex, C., Marjo, C.E., Markowska, M., and Rau, G.C. 2015. Organic characterisation of cave drip water by LC-OCD and fluorescence analysis. *Geochimica et Cosmochimica Acta,* 166, 15-26.

Sharp, Z., 2007. *Principles of Stable Isotope Geochemistry*. Pearson Prentice Hall, Upper Saddle River, NJ.

Sheffer, N.A., Cohen, M., Morin, E., Grodek, T., Gimburg, A., Magal., E., Gvirtzman, H., Nied, M., Isele, D., Frumkin, A. 1998. Integrated cave drip monitoring for epikarst recharge estimation in a dry Mediterranean area, Sif Cave, Israel, Hydrological Processes, 25, 2837-2845.

Smart, P.L. & Friederich H., 1986. Water movement and storage in the unsaturated zone of a maturely karstified carbonate aquifer, Mendip Hills, England. *Proceedings of the Environmental Problems in Karst Terranes and their Solutions Conference*, KY, 59-87.

Tooth A.F. & Fairchild I.J., 2003. Soil and karst aquifer hydrologic controls on the geochemical evolution of speleothem-forming drip waters, Crag Cave, southwest Ireland. *Journal of Hydrology*, 273: 51–68.

Trabucco, A., and Zomer, R.J. 2009. Global Aridity Index (Global-Aridity) and Global Potential Evapo-Transpiration (Global-PET) Geospatial Database. CGIAR Consortium for Spatial Information. Published online, available from the CGIAR-CSI GeoPortal at: http://www.csi.cgiar.org/

Treble, P. C., Bradley, C., Wood, A., Baker, A., Jex, C. N., Fairchild, I. J., Gagan M.J., Cowley, J., & Azcurra, C. 2013. An isotopic and modelling study of flow paths and storage in Quaternary calcarenite, SW Australia: implications for speleothem paleoclimate records. *Quaternary Science Reviews*, 64, 90-103.

UNEP (1992). *World Atlas of Desertification*. United Nations Environment Programme. London, UK

Vacher, H.L.,Mylroie J.E. 2002. Eogenetic karst from the perspective of an equivalent porous medium. *Carbonates and Evaporates*, 17(2), 182-196.

Vaks, A., Bar-Matthews, M., Matthews, A., Ayalon, A., Frumkin, A. 2010. Middle-Late Quaternary paleoclimate of northern margins of the Saharan-Arabian Desert: reconstruction from speleothems of Negev Desert, Israel, Quaternary Science Reviews, 29(19–20), 2647-2662.

van Beynen, P. and Febbroriello, P.2006. Seasonal isotopic variability of precipitation and cave drip water at Indian Oven Cave, New York. *Hydrological Processes*, 20, 1793–1803.

Verheyden, S., Genty, D., Deflandre, G., Quinif, Y., Keppens. E. 2008. Monitoring climatological, hydrological and geochemical parameters in the Père Noël cave (Belgium): implication for the interpretation of speleothem isotopic and geochemical time-series. *International Journal of Speleology*, 37: 221-234.

Vickers, A.J. 2005. Parametric versus non-parametric statistics in the analysis of randomized trials with non-normally distributed data. *BMC Medical Research Methodology*,5:35 doi:10.1186/1471-2288-5-35

Walton, K. 1969. *The Arid Zones*. Aldine Transaction, New Brunswick, USA.

Wang, Y., Cheng, H., Edwards, R.L., An, Z., Wu, J., Shen, C., Dorale, J.A., 2001, A high-resolution absolute-dated late Pleistocene monsoon record from Hulu Cave, China. *Science*, 294, 2345–2348.

Williams, P.W. 2008. The role of the epikarst in karst and cave hydrogeology: a review. *International Journal of Speleology*. 37(1)1–10.

Williams P.W. & Fowler A., 2002 - Relationship between oxygen isotopes in rainfall, cave percolation waters and speleothem calcite at Waitomo, New Zealand. New Zealand. *Journal of Hydrology*, 41(1): 53–70.

Yonge, C. J., Ford, D. C., Gray, J., & Schwarcz, H. P. 1985. Stable isotope studies of cave seepage water. *Chemical Geology: Isotope Geoscience section*, 58(1), 97-105.

Figure 1

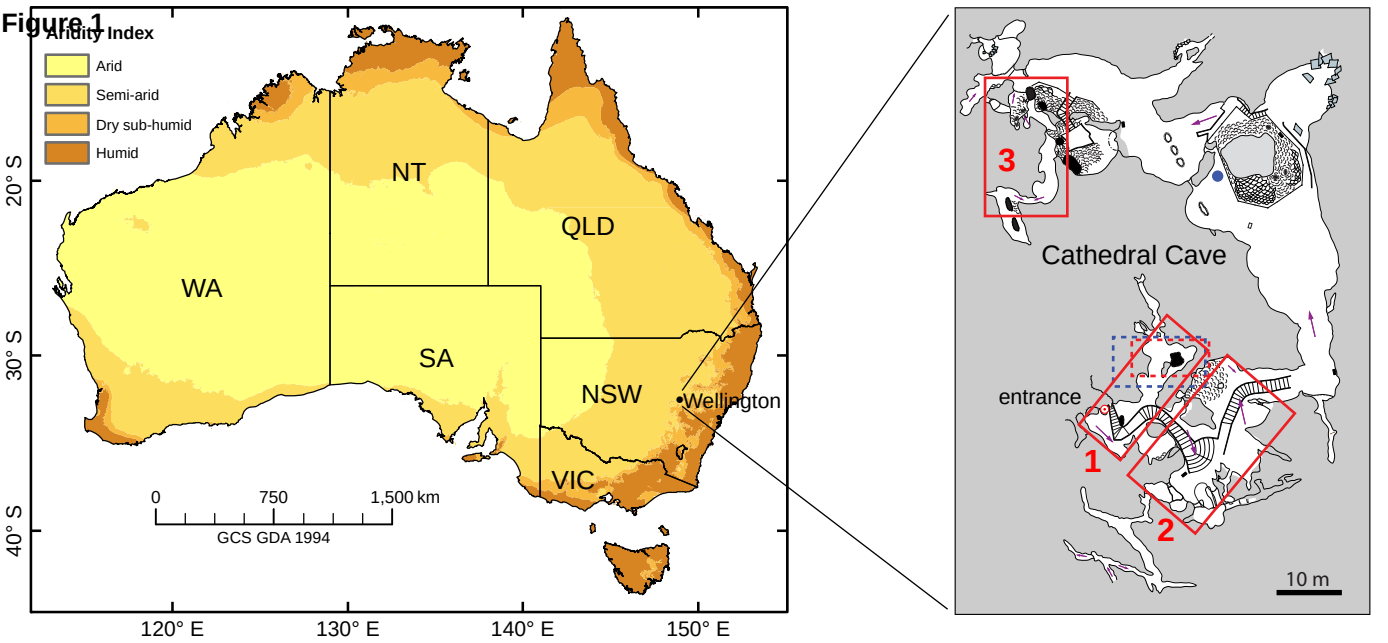

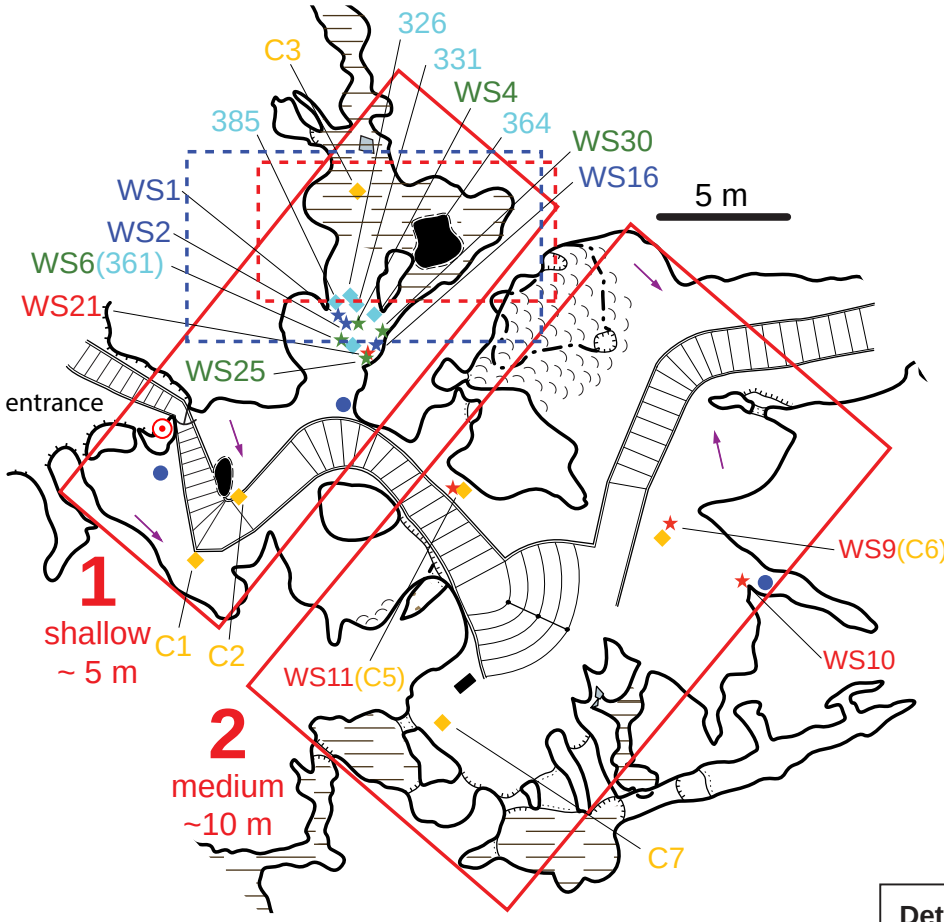

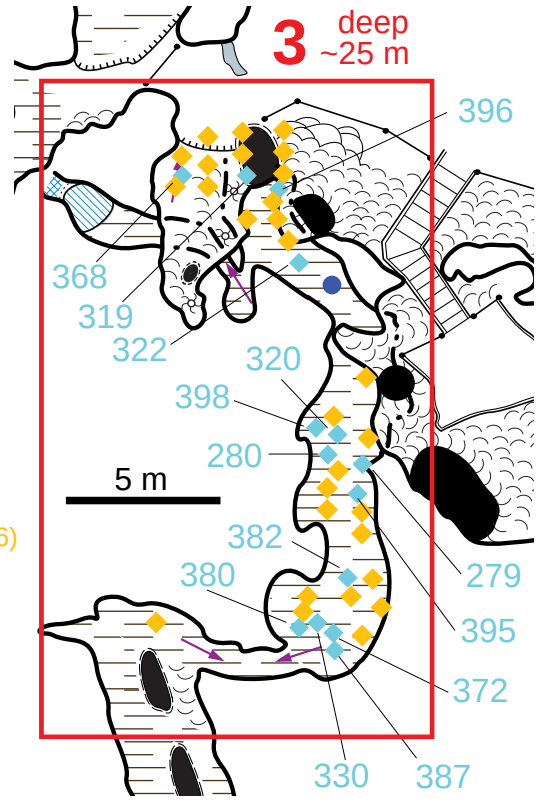

General cave features:

- Formed track, stairs
- Handrail, junction box
- Flowstone, rimstone
- Column, stalactite, stalagmite
- Gravel, mud
- Lake, underwater passage
- Down slope

Details of current investigation:

- 2013 surface irrigation
- 2014 surface irrigation
- 2013 irrigation samples
- 2014 irrigation samples
- 2013/2014 irrigation samples
- Monthly integrated samples 2011-2013
- Spot samples 2010-2011
- Evaporation pans
- Benchmark at 681998.559 m East and 6388990.647 m North (Zone 55) Elevation at approx. 325.07 mAHD (based on GDA94)

Figure 2

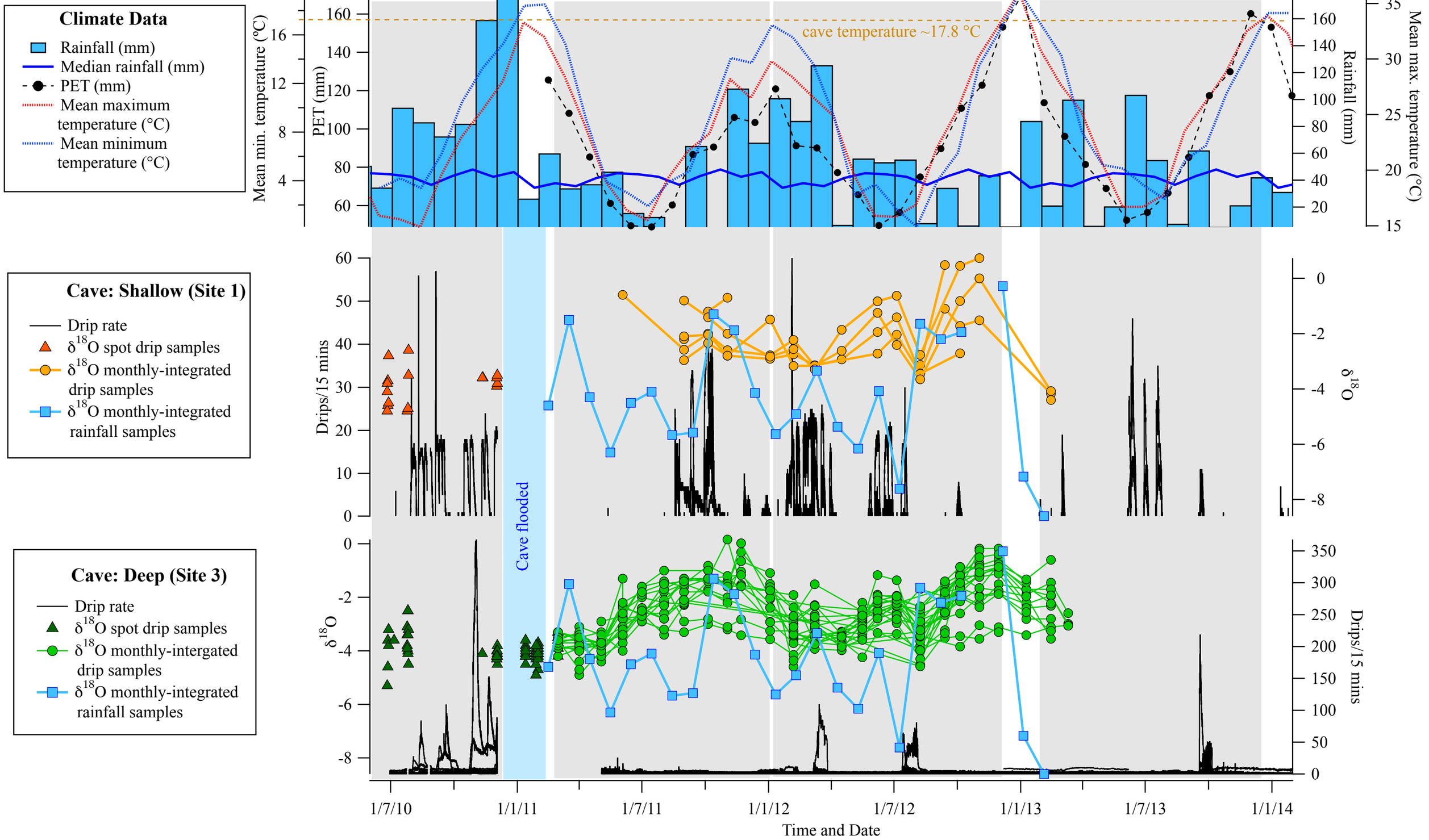
Climate Data
Rainfall (mm)
Median rainfall (mm)
PET (mm)
Mean maximum temperature (°C)
Mean minimum temperature (°C)
cave temperature ~17.8 °C
Mean min. temperature (ºC)
PET (mm)
Rainfall (mm)
Mean max. temperature (°C)
Cave: Shallow (Site 1)
Drip rate
δ18O spot drip samples
δ18O monthly-integrated drip samples
δ18O monthly-integrated rainfall samples
Drips/15 mins
δ18O
Cave flooded
Cave: Deep (Site 3)
Drip rate
δ18O spot drip samples
δ18O monthly-intergated drip samples
δ18O monthly-integrated rainfall samples
δ18O
Drips/15 mins
1/7/10
1/1/11
1/7/11
1/1/12
1/7/12
1/1/13
1/7/13
1/1/14
Time and Date

Figure 3A

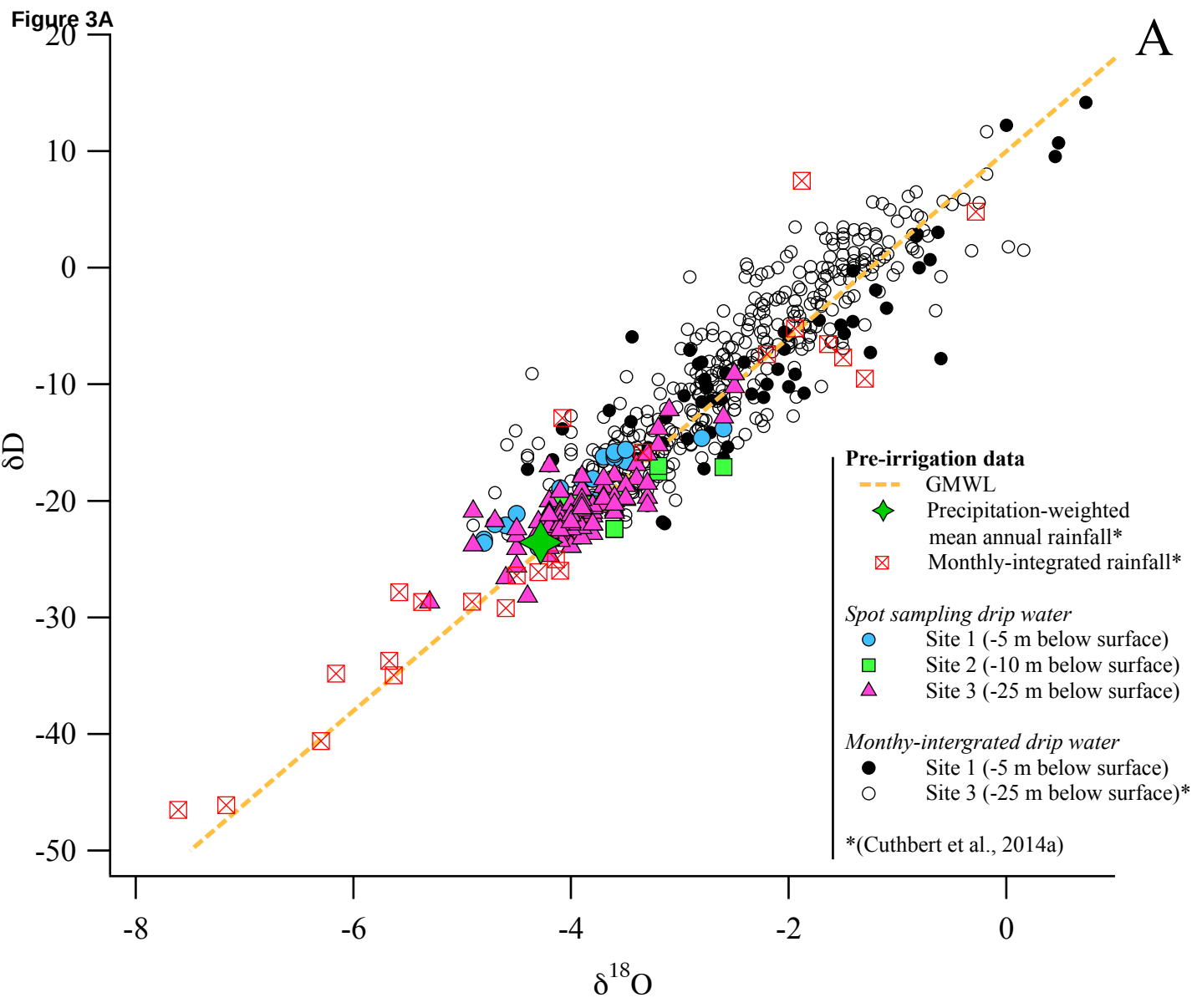
A
20
10
0
-10
-20
-30
-40
-50
δD
-8
-6
-4
-2
0
δ18O
Pre-irrigation data
GMWL
Precipitation-weighted mean annual rainfall*
Monthly-integrated rainfall*
Spot sampling drip water
Site 1 (-5 m below surface)
Site 2 (-10 m below surface)
Site 3 (-25 m below surface)
Monthy-intergrated drip water
Site 1 (-5 m below surface)
Site 3 (-25 m below surface)*
*(Cuthbert et al., 2014a)

Figure 3B **Pre-irrigation data**

B

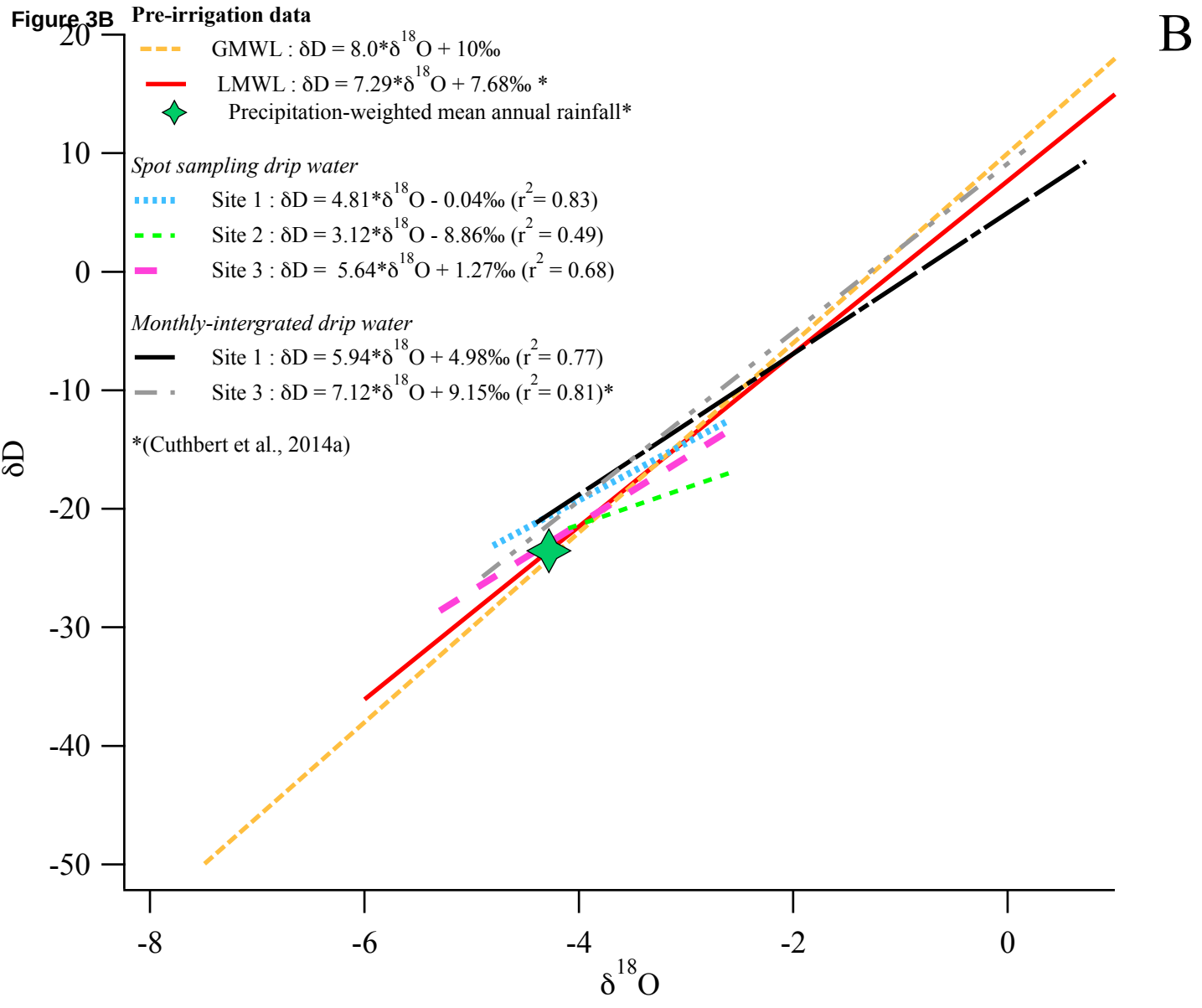

Figure 4

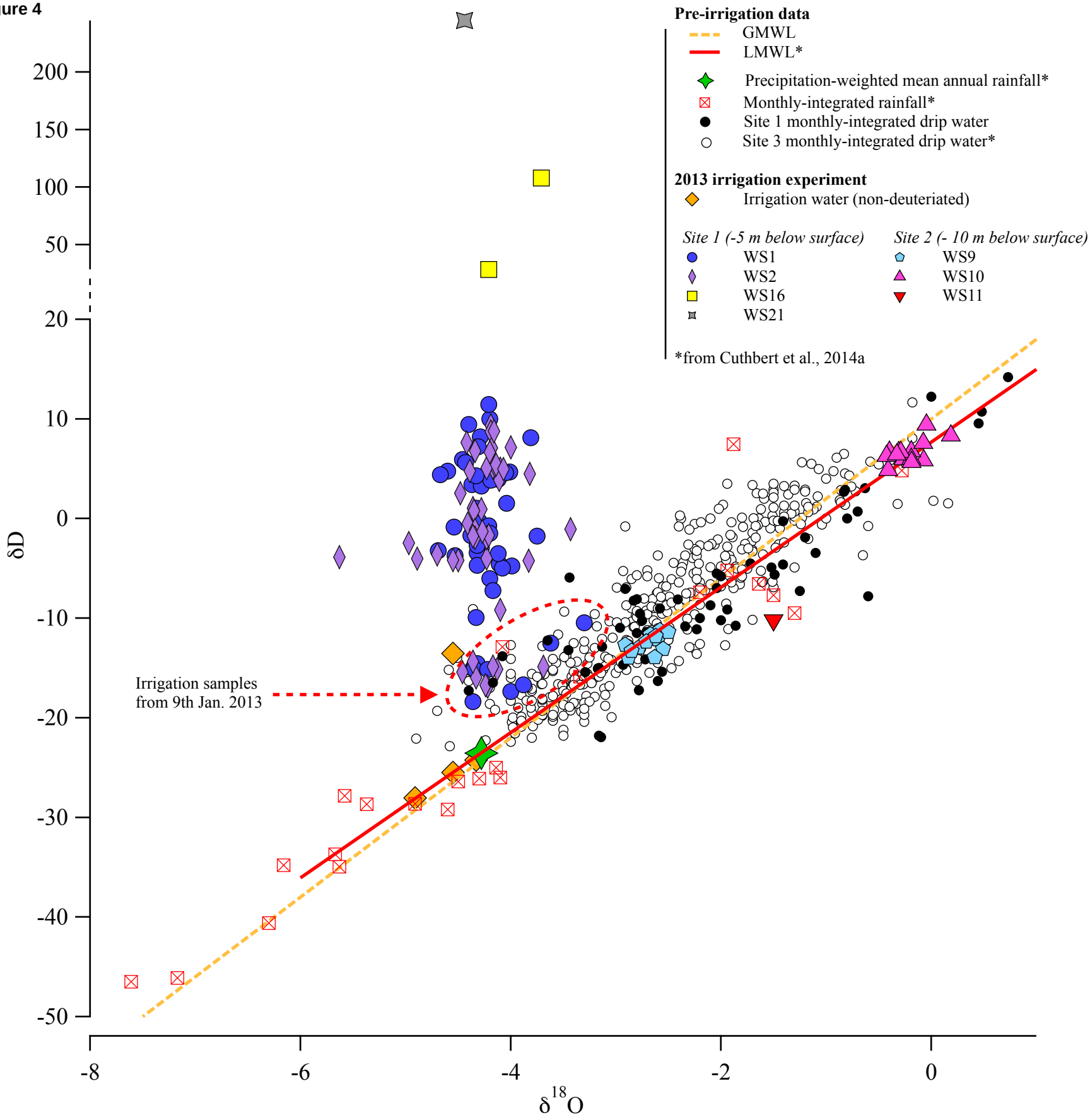
Pre-irrigation data
GMWL
LMWL*
Precipitation-weighted mean annual rainfall*
Monthly-integrated rainfall*
Site 1 monthly-integrated drip water
Site 3 monthly-integrated drip water*
2013 irrigation experiment
Irrigation water (non-deuteriated)
Site 1 (-5 m below surface)
WS1
WS2
WS16
WS21
Site 2 (- 10 m below surface)
WS9
WS10
WS11
*from Cuthbert et al., 2014a
Irrigation samples
from 9th Jan. 2013
δD
δ18O
200
150
100
50
20
10
0
-10
-20
-30
-40
-50
-8
-6
-4
-2
0

Figure 5

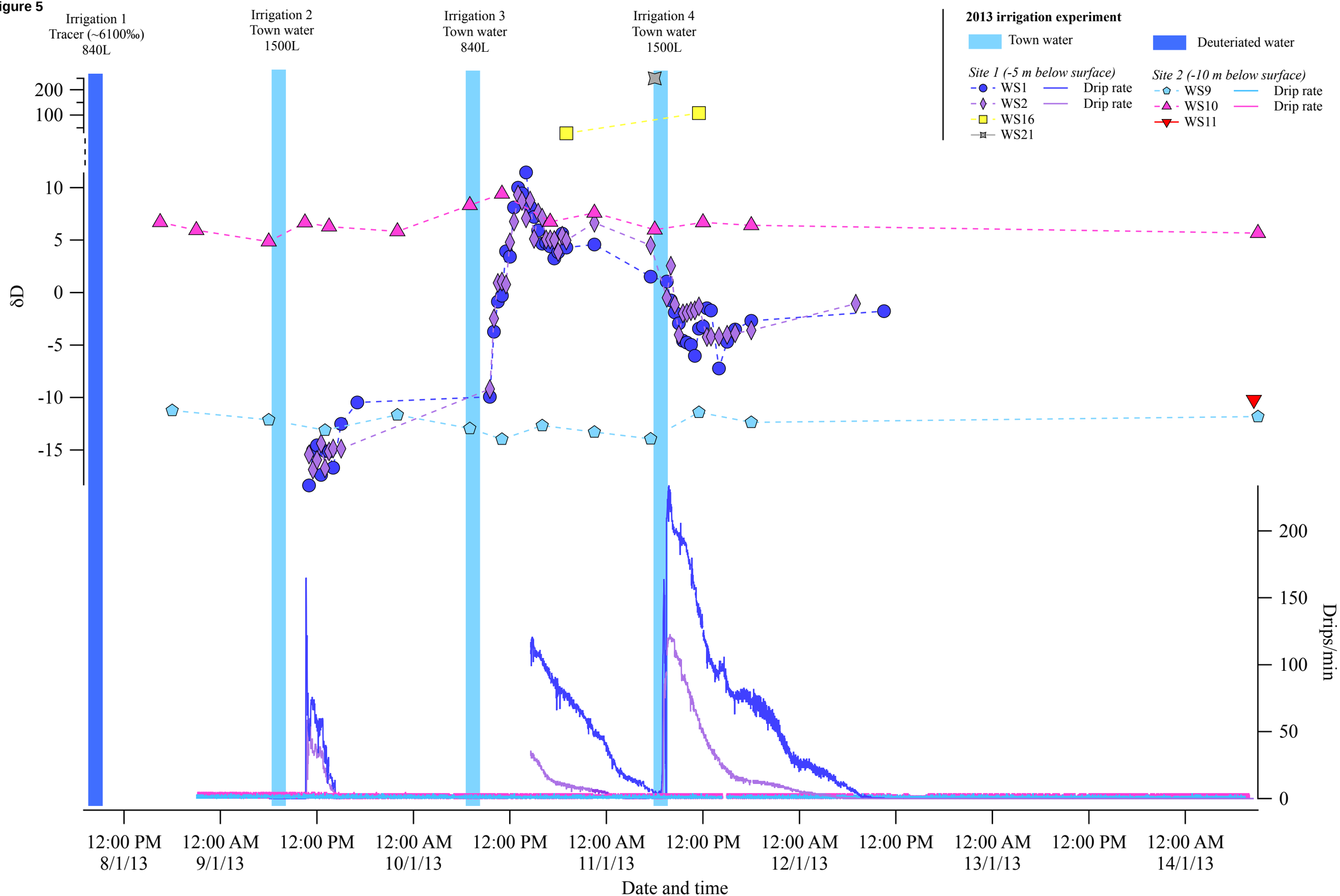
Irrigation 1
Tracer (~6100‰)
840L
Irrigation 2
Town water
1500L
Irrigation 3
Town water
840L
Irrigation 4
Town water
1500L
2013 irrigation experiment
Town water
Deuteriated water
Site 1 (-5 m below surface)
WS1
WS2
WS16
WS21
Drip rate
Drip rate
Site 2 (-10 m below surface)
WS9
WS10
WS11
Drip rate
Drip rate
δD
200
100
10
5
0
-5
-10
-15
200
150
100
50
0
Drips/min
12:00 PM 8/1/13
12:00 AM 9/1/13
12:00 PM
12:00 AM 10/1/13
12:00 PM
12:00 AM 11/1/13
12:00 PM
12:00 AM 12/1/13
12:00 PM
12:00 AM 13/1/13
12:00 PM
12:00 AM 14/1/13
Date and time

Figure 6

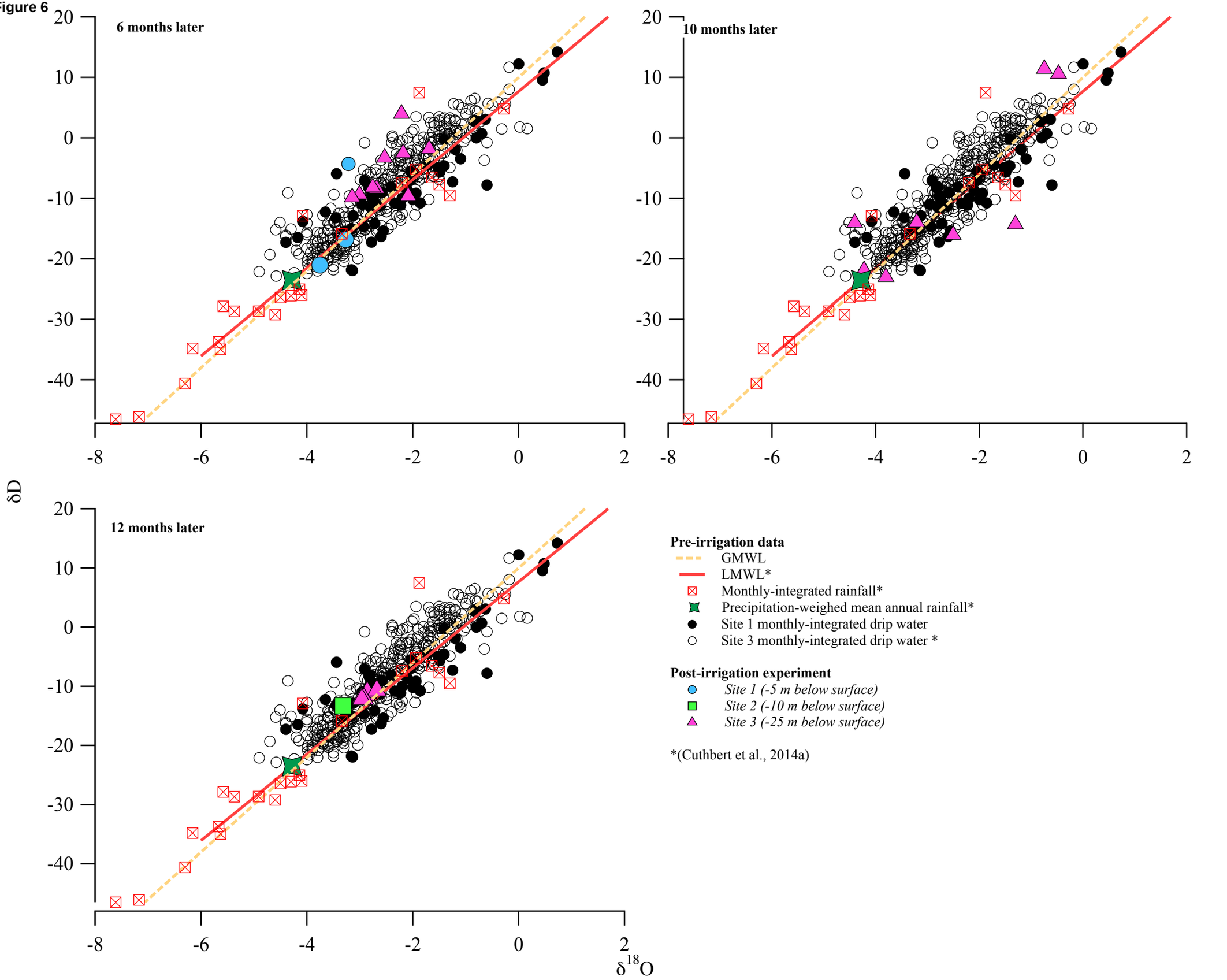
6 months later
10 months later
12 months later
δD
δ18O
20
10
0
-10
-20
-30
-40
-8
-6
-4
-2
0
2
Pre-irrigation data
GMWL
LMWL*
Monthly-integrated rainfall*
Precipitation-weighed mean annual rainfall*
Site 1 monthly-integrated drip water
Site 3 monthly-integrated drip water *
Post-irrigation experiment
Site 1 (-5 m below surface)
Site 2 (-10 m below surface)
Site 3 (-25 m below surface)
*(Cuthbert et al., 2014a)

Figure 7

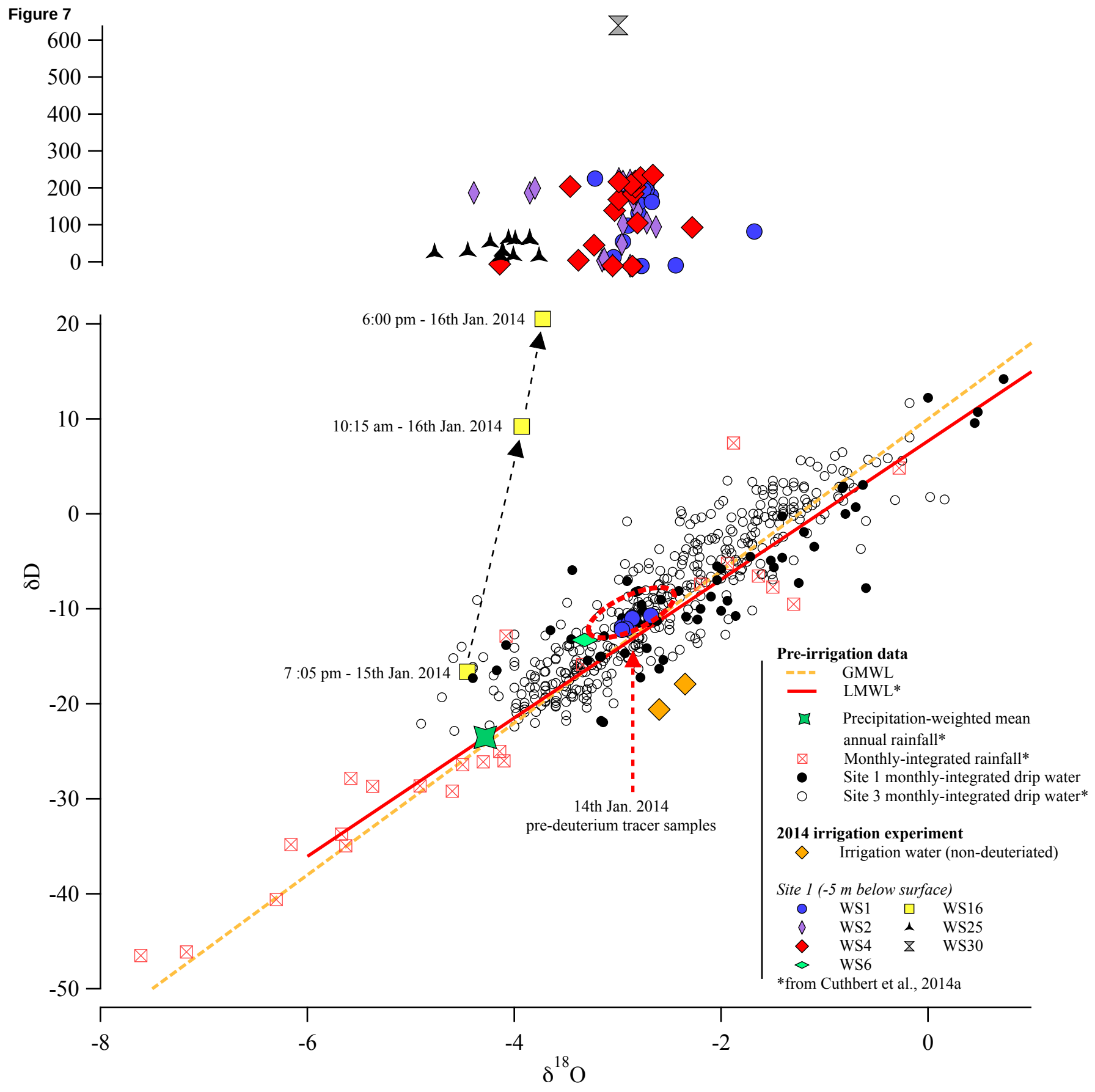
600
500
400
300
200
100
0
20
10
0
-10
-20
-30
-40
-50
δD
-8
-6
-4
-2
0
δ18O
6:00 pm - 16th Jan. 2014
10:15 am - 16th Jan. 2014
7 :05 pm - 15th Jan. 2014
14th Jan. 2014
pre-deuterium tracer samples
Pre-irrigation data
GMWL
LMWL*
Precipitation-weighted mean annual rainfall*
Monthly-integrated rainfall*
Site 1 monthly-integrated drip water
Site 3 monthly-integrated drip water*
2014 irrigation experiment
Irrigation water (non-deuteriated)
Site 1 (-5 m below surface)
WS1
WS2
WS4
WS6
WS16
WS25
WS30
*from Cuthbert et al., 2014a

Figure 8

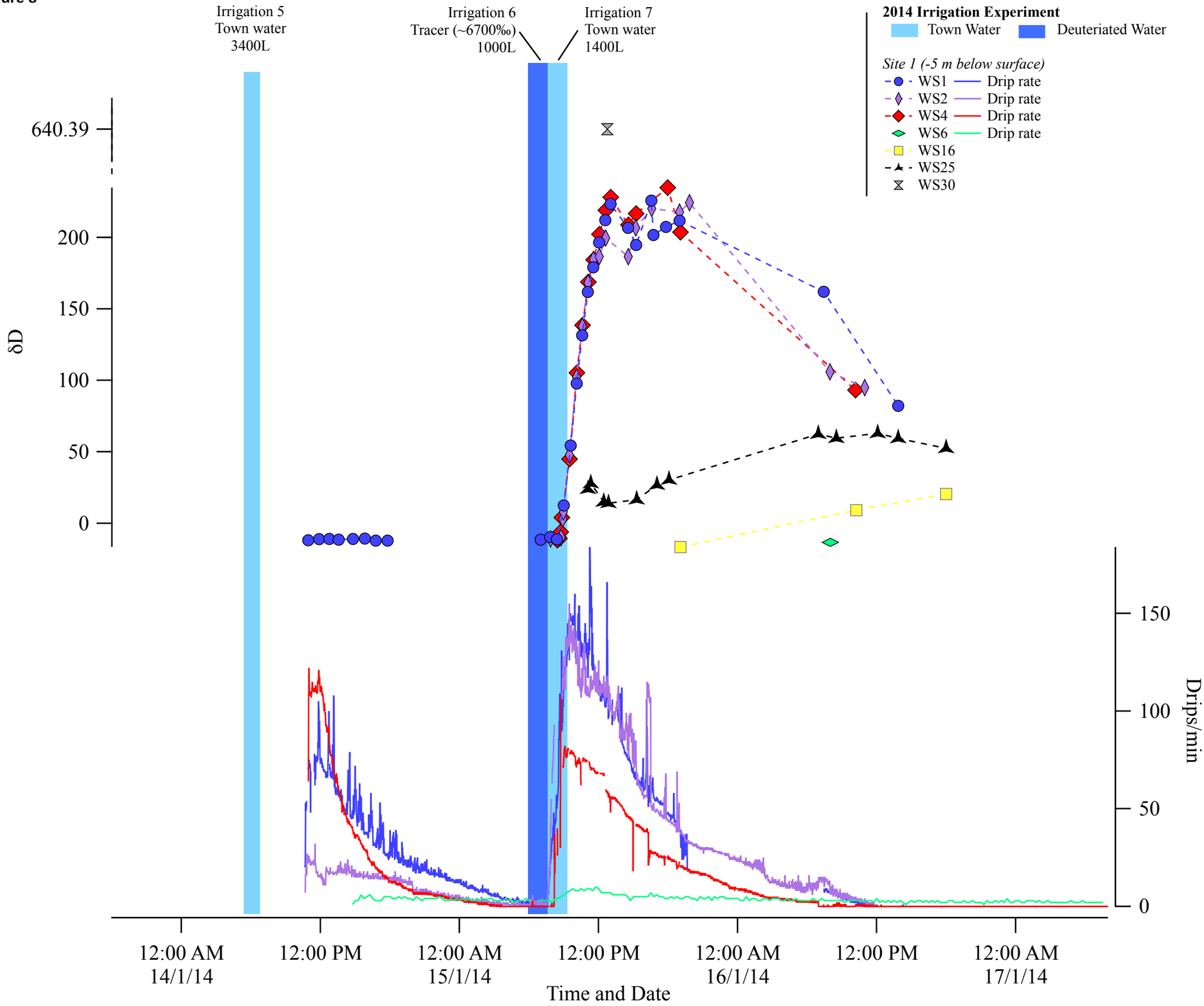
Irrigation 5
Town water
3400L
Irrigation 6
Tracer (~6700‰)
1000L
Irrigation 7
Town water
1400L
2014 Irrigation Experiment
Town Water
Deuteriated Water
Site 1 (-5 m below surface)
WS1
Drip rate
WS2
Drip rate
WS4
Drip rate
WS6
Drip rate
WS16
WS25
WS30
640.39
200
150
100
50
0
δD
150
100
50
0
Drips/min
12:00 AM
14/1/14
12:00 PM
12:00 AM
15/1/14
12:00 PM
12:00 AM
16/1/14
12:00 PM
12:00 AM
17/1/14
Time and Date

Figure 9

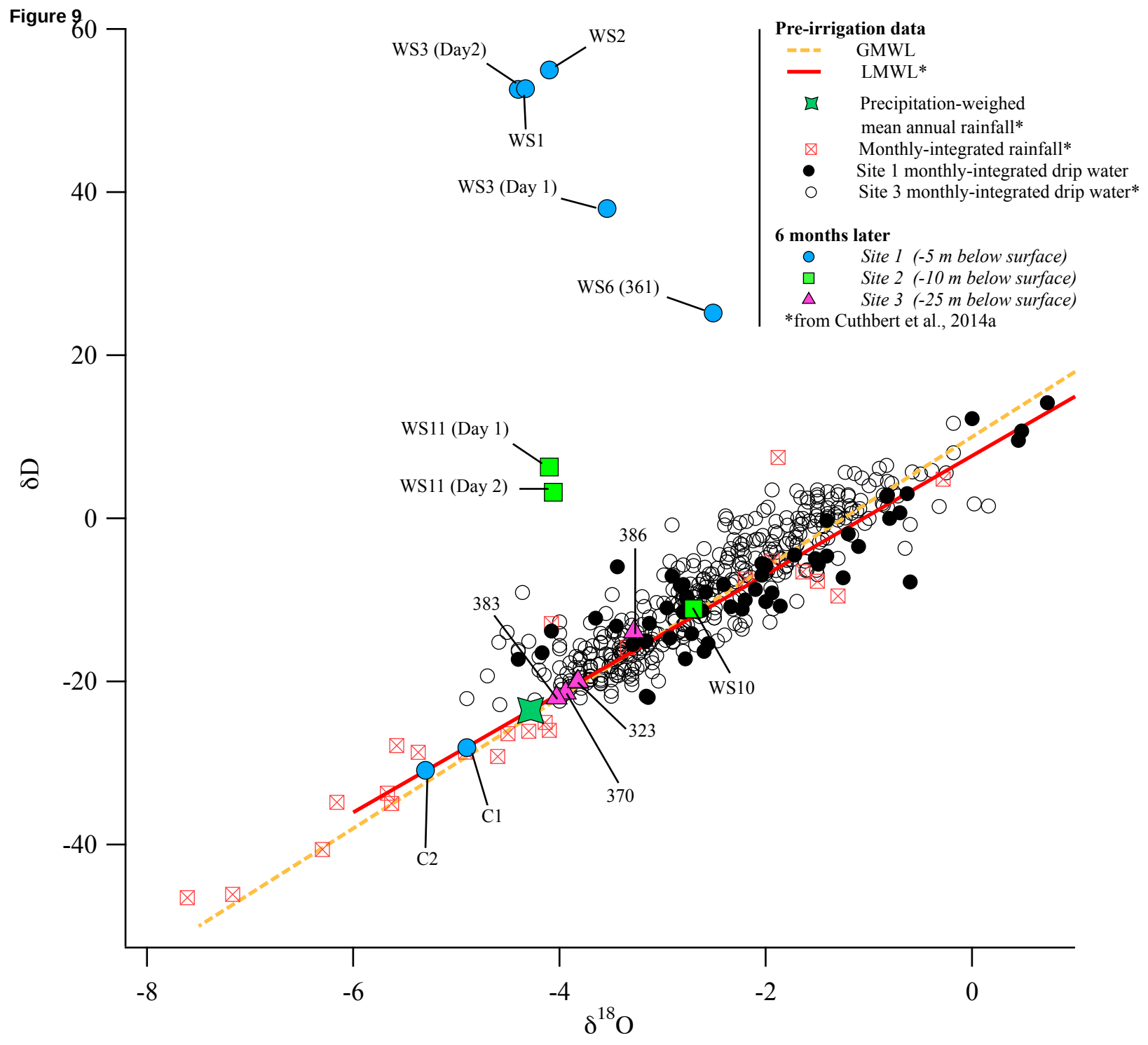
Pre-irrigation data
GMWL
LMWL*
Precipitation-weighed mean annual rainfall*
Monthly-integrated rainfall*
Site 1 monthly-integrated drip water
Site 3 monthly-integrated drip water*
6 months later
Site 1 (-5 m below surface)
Site 2 (-10 m below surface)
Site 3 (-25 m below surface)
*from Cuthbert et al., 2014a
WS3 (Day2)
WS2
WS1
WS3 (Day 1)
WS6 (361)
WS11 (Day 1)
WS11 (Day 2)
386
383
WS10
323
370
C1
C2
δD
δ18O
60
40
20
0
-20
-40
-8
-6
-4
-2
0

Figure captions

Figure 1. Aridity map of Australia compiled with spatial aridity data from Trabucco and Zomer (2009) (top left). Plan-view map of Cathedral Cave with cave sites 1 to 3 marked (top right). An expanded plan-view of sites 1 and 2, marked with irrigation areas and drip sampling points (middle left). An expanded plan-view of site 3 with pre-irrigation drip sampling points (right middle). Legend of general cave features and details of current investigation (bottom). Map adapted from Sydney Speleological Survey Map, 2006.

Figure 2. Monthly total rainfall, median rainfall, mean minimum temperature and mean maximum temperature (observations from years 1881-2014) over the cave monitoring period from Bureau of Meteorology station 065034 Wellington Agrowplow (BOM, 2014). PET was calculated using the Penman-Monteith equation on data for a nearby site (Wellington UNSW Research Station) and extended using a derived pan factor correlation with monthly Australian Government Bureau of Meteorology evaporation pan data for station Agrowplow (065034) (BOM, 2014). Drip rate (drips/15 mins) and water monitoring at Site 1 (- 5 m below the surface) and Site 3 (South Passage, 25 m below the surface; from Cuthbert et al., 2014a) over 2010-2013. Note that the cave flooded during early 2011 and no drip data exists for this period. The grey bars indicate periods most likely to result in calcite precipitation based on temperature differences inside (~17.8 °C) and outside (mean minimum temperature °C). A sampling timeline is shown at the top of the figure, outlining the timing of pre-irrigation and irrigation sampling.

Figure 3. Panel A: Spot sampling over the period 2010-2011 is shown at three sampling locations (site 1, 2 and 3) with monthly-integrated sampling data over the period 2011-2013 (black and open circles) from two sampling locations (site 1 and 3). The Global Meteoric Waterline (GMWL) is shown (yellow dashed line) as well as the monthly-integrated rainfall data (square red crosses) over the period 2011-2013 and the precipitation-weighed mean annual rainfall (green diamond) (Cuthbert et al., 2014a). Panel B: Regression lines for the above data are shown here with corresponding regression equations as well as the Local Meteoric Waterline and precipitation-weighted mean annual rainfall from Cuthbert et al. (2014a).

Figure 4. δD vs $\delta^{18}O$ plot from 2013 irrigation experiment with drip water results from sites 1 and 2. Site 3 did not respond during the irrigation. Irrigation water not spiked with deuterium is also shown (yellow diamonds). The red dashed line encircles drip waters discharges from WS1 and WS2 after irrigation 2. Background pre-irrigation data from monthly-integrated monitoring is shown for context (black and open circles), as well as the GMWL (yellow dashed line) and LMWL (red solid line) and monthly-integrated rainfall sampling and precipitation-weighted mean annual rainfall (green diamond) from Cuthbert et al. (2014a).

Figure 5. Time series of drip rate (drips/min) and δD (‰) from the 2013 irrigation experiment are plotted over the 7-day monitoring period for sites 1 and 2. Thick blue bars denote irrigation periods. Deep blue bar denotes irrigation spiked with deuterium (~6100‰). Note that WS21 activated after irrigation 3 and the water sample was from an overnight collection.

Figure 6. Post-irrigation sampling during 6 months, 10 months and 12 months after the 2013 irrigation experiment at sites 1, 2 and 3. Pre-irrigation data including monthly-integrated isotopic sampling from sites 1 and 3 (Cuthbert et al, 2014a), GMWL (yellow dashed line) and from Cuthbert et al. (2014a) monthly-integrated rainfall (square red crosses), precipitation-weighed mean annual rainfall (green diamond), and LMWL (red solid line) are included for context.

Figure 7. δD vs $\delta^{18}O$ plot from 2014 irrigation experiment with drip water results from sites 1. Sites 2 and 3 did not respond during the irrigation. Irrigation water not spiked with deuterium is also shown (yellow diamonds). The time evolution of drip WS16 is indicated by the times and dashed arrows. The red dashed line encircles drip waters discharges from WS1 prior to tracer addition. Background pre-irrigation data from monthly-integrated monitoring is shown for context (black and open circles), as well as the GMWL (yellow dashed line) and LMWL (red solid line) and monthly-integrated rainfall sampling (square red crosses) and precipitation-weighted mean annual rainfall (green diamond) from Cuthbert et al. (2014a).

Figure 8. Time series of drip rate (drips/min) and δD (‰) from the 2014 irrigation experiment are plotted over the 3-day monitoring period for site 1. Thick blue bars denote irrigation periods. Deep blue

bar denotes irrigation spiked with deuterium (~6700‰). Note that WS6 activated after irrigation 7 and the water sample was from an overnight collection.

Figure 9. Post-irrigation sampling from the 2014 irrigation experiment 6 months later. Deuterium tracer evident at from drips at sites 1 and 2, but not 3. Pre-irrigation data including monthly-integrated isotopic sampling from sites 1 and 3 (Cuthbert et al, 2014a), GMWL (yellow dashed line) and from Cuthbert et al. (2014a) monthly-integrated rainfall (square red crosses), precipitation-weighed mean annual rainfall (green diamond), and LMWL (red solid line) are included for context..